Journal of Medicinal Chemistry

Article

Discovery of N-[4-(quinolin-4-yloxy)-phenyl]-benzenesulfonamides as novel AXL kinase inhibitors

István Szabadkai, Robert Torka, Rita Garamvölgyi, Ferenc Baska, Pál Gyulavári, Sándor Boros, Eszter Illyés, Axel Choidas, Axel Ullrich, and László #rfi

J. Med. Chem., **Just Accepted Manuscript** • DOI: 10.1021/acs.jmedchem.8b00672 • Publication Date (Web): 21 Jun 2018

Just Accepted

ACS Publications

is published by the American Chemical Society. 1155 Sixteenth Street N.W., Washington, DC 20036

Discovery of *N*-[4-(quinolin-4-yloxy)-phenyl]-benzenesulfonamides as novel AXL kinase inhibitors

István Szabadkai[†,⊥], Robert Torka[#,⊥], Rita Garamvölgyi[†,∞], Ferenc Baska[†], Pál Gyulavári[#], Sándor Boros[†], Eszter Illyés[†], Axel Choidas[∫], Axel Ullrich[‡], László Őrfi[*,†,∞]

[†]Vichem Chemie Research Ltd., Budapest, Hungary

[#]Institute of Physiological Chemistry, University Halle-Wittenberg, Halle (Saale), Germany

[‡]Department of Molecular Biology, Max Planck Institute of Biochemistry, Martinsried, Germany

[∫]Lead Discovery Center GmbH, Dortmund, Germany

[∞]Department of Pharmaceutical Chemistry, Semmelweis University, Budapest, Hungary

ABSTRACT

The overexpression of AXL kinase has been described in many types of cancer. Due to its role in proliferation, survival, migration and resistance AXL represents a promising target in the treatment of the disease. In this study we present a novel compound family which successfully targets the AXL kinase. Through optimization and detailed SAR studies we developed low nanomolar inhibitors and after further biological characterization we identified a potent AXL kinase inhibitor with favorable pharmacokinetic profile. The antitumor activity was determined in xenograft models and the lead compounds reduced the tumor size by 40% with no observed toxicity as well as lung metastasis formation by 66% when compared to vehicle control.

KEYWORDS

AXL kinase, inhibitor, metastasis, antitumor agents, cancer, *N*-[4-(quinolin-4-yloxy)-phenyl]-benzenesulfonamides.

INTRODUCTION

Receptor tyrosine kinases (RTKs) are transmembrane proteins, linking the extra- and intracellular environment. As mediators of signal transduction, they play a major role in normal cellular processes, including differentiation, proliferation, adhesion, migration, apoptosis and metabolism.

A subfamily of mammalian RTKs is called TAM family, including AXL, MER and TYRO-3. AXL was originally identified in chronic myelogenous leukemia (CML)[1] and chronic myeloproliferative disorder.[2] Subsequently, its overexpression has been reported in many human cancers, comprising breast, lung, prostate, colon, esophageal, liver and other, which have been reviewed by Paccez et al.[3]

AXL can primarily be stimulated by Gas6 (Growth arrest-specific 6).[4] As a result of the activation of AXL kinase, various signaling pathways can be activated, such as phosphoinositide 3-kinase (PI3K), including AKT, S6K[5] or NF-κB[6] as downstream targets, mitogen-activated protein kinase (MAPK) pathway[7] or signal transducer and activator of transcription (STAT).[8] Aberrant regulation of Gas6/AXL signaling contribute to cell proliferation, increased cell survival, migration and angiogenesis,[9] therefore they play an important role in oncogenic transformation, metastasis and tumor growth. AXL may be a biomarker of resistance in targeted therapy-resistant cancers.[10]

According to its central role in neoplastic processes, the AXL signaling pathway represents a notable molecular therapeutic target in the fight against cancer. A number of agents inhibiting

the biological activity of AXL has been described in the literature (Figure 1), e.g. amuvatinib (MP-470) (**1**),[11] bosutinib (SKI-606) (**2**),[12] foretinib (XL880) (**3**),[13] BMS-777607 (**4**),[14] cabozantinib (XL184) (**5**)[15] or S49076 (**6**).[16] However, most of these small molecule kinase inhibitors were developed against other targets, such as cKIT, SRC/ABL, c-MET or VEGFR-2. The first selective inhibitor developed purposely to target AXL kinase was compound R428 (**7**).[17]

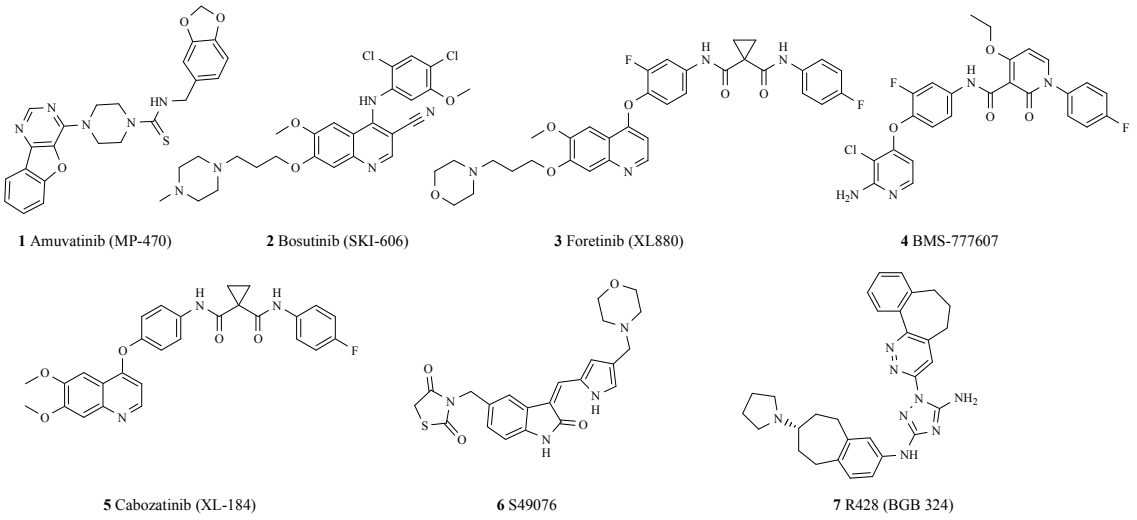

Figure 1. Structures of reported small-molecule tyrosine kinase inhibitors exhibiting activity against AXL kinase

We have applied Vichem's Nested Chemical Library™ technology[18] to discover hit compounds against AXL kinase. As we previously reported, bosutinib (**2**) was found to inhibit the AXL kinase activity in a dose dependent manner, with an IC_{50} of 0.56 μM.[12] The 4-phenoxyquinoline derivative (Figure 2) Ki8751 (**8**) was originally developed by Kubo et al.[19] as a VEGFR-2 tyrosine kinase inhibitor. Since structural similarity can be found between bosutinib (**2**) and Ki8751 (**8**), it was practical to determine the AXL kinase inhibitory effect of Ki8751 (**8**), which was found to be even better (IC_{50} = 0.30 μM) than that of bosutinib (**2**).

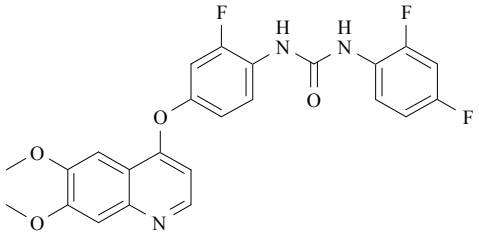

8 Ki8751

Figure 2. Structure of an *N*-phenyl-*N'*-{4-(4-quinolyloxy)phenyl}urea derivative

In this manuscript, we present a novel *N*-[4-(quinolin-4-yloxy)-phenyl]-benzenesulfonamide series we have designed to target AXL kinase, describe their synthesis, biological activity and structure-activity relationships.

Chemical Synthesis

(All chemical synthesis procedures are described in detail in the Supporting Information.) The *N*-[4-(6,7-dimethoxy-quinolin-4-yloxy)-phenyl]-benzenesulfonamide derivatives (**12a-12u**) were prepared according to the general synthetic route shown in Scheme 1.

Scheme 1. Synthesis of *N*-[4-(6,7-dimethoxy-quinolin-4-yloxy)-phenyl]-benzenesulfonamide derivatives [a]

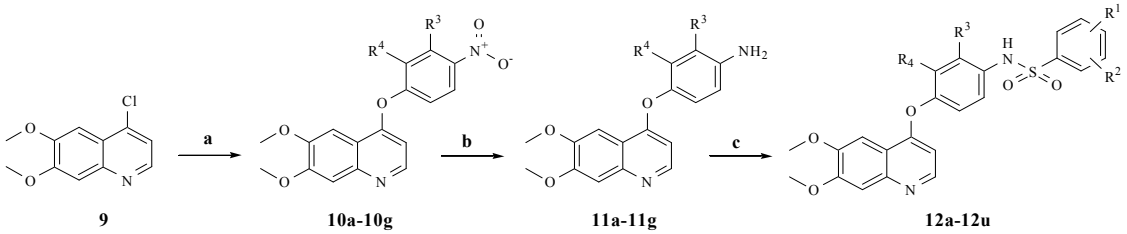

9 **10a-10g** **11a-11g** **12a-12u**

[a] Reagents and conditions: (a) 4-nitrophenols, chlorobenzene, DIPEA, reflux, 2 days; (b) Zn, NH_4Cl, $EtOH/H_2O$, reflux, 3 hours; (c) benzenesulfonyl chlorides, pyridine, rt, 2 days.

The starting material (4-chloro-6,7-dimethoxy-quinoline, **9**) was commercially available. This compound was coupled with various 4-nitrophenols by heating them in chlorobenzene, in the presence of *N,N*-diisopropylethylamine (DIPEA). The isolated 4-(4-nitro-phenoxy)-quinoline compounds (**10a-10g**) were reduced by zinc powder and ammonium chloride in ethanol/water mixture at reflux temperature. The coupling reaction of the anilines (**11a-11g**) with benzenesulfonyl chlorides in pyridine provided the corresponding sulfonamide derivatives (**12a-12u**).

In order to introduce alkoxy side chains containing amino- or ester groups into the positions 6 and 7 of the quinoline ring, required the protection of the hydroxyl group. The general synthetic route for the preparation of these compounds is shown in Scheme 2.

Scheme 2. Synthesis of *N*-[4-(substituted-quinolin-4-yloxy)-phenyl]-benzenesulfonamide derivatives bearing a side chain (R^7) [a]

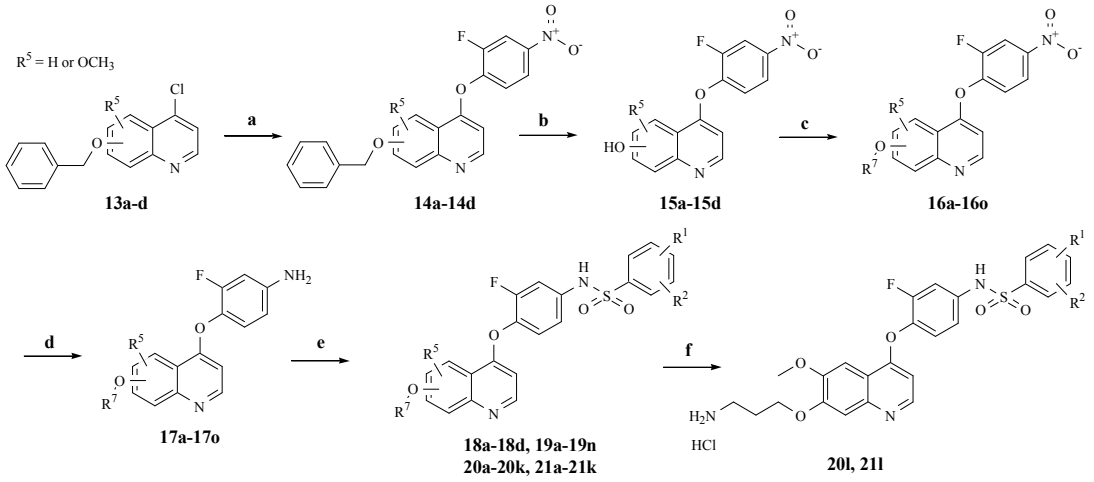

[a] Reagents and conditions: (a) 4-nitrophenols, chlorobenzene, reflux, 2 days; (b) 33% HBr solution, rt, 2 hours; (c) alkyl halogenides, acetonitrile, Cs_2CO_3, KI, rt, 45 min, then reflux 3 hours; (d) Zn, NH_4Cl, $EtOH/H_2O$, reflux, 3 hours; (e) benzenesulfonyl chlorides, pyridine, 60 °C, 3 days, (f) transformation of **20k** and **21k**, HCl, ethyl acetate, rt, 3 hours.

The starting materials (4-chloro-benzyloxy-quinoline derivatives, **13a-13d**) were available from commercial sources. These benzyloxy-4-chloroquinoline derivatives (**13a-13d**) were coupled with 2-fluoro-4-nitrophenol by heating them in chlorobenzene in the presence of *N,N*-diisopropylethylamine. The benzyloxy protective group was removed from the isolated 4-(4-nitro-phenoxy)-quinoline compounds (**14a-14d**) by hydrobromic acid in acetic acid. The obtained hydroxy-quinolines (**15a-15d**) were alkylated by the proper alkyl halogenides resulting in the appropriate alkoxy derivatives (**16a-16o**). The reduction of the nitro groups of these compounds was carried out by zinc powder and ammonium chloride in ethanol/water mixture at reflux temperature, whereas the coupling of (**17a-17o)** with benzenesulfonyl chlorides in pyridine gave the desired sulfonamides (**18a-18d**, **19a-19n**, **20a-20k** and **21a-21k**) as final products. In the case of **20k** and **21k**, after removing the tert-butoxycarbonyl (BOC) protecting group we isolated the aminopropoxy derivatives as hydrochloride salt (**20l** and **21l**).

RESULTS AND DISCUSSION

The compounds prepared for this study were primarily evaluated by *in vitro* AXL kinase assay. In order to determine the structure-activity relationships, the following moieties were changed: substituents of the benzenesulfonamide ring (R^1, R^2), substituents of the *p*-aminophenol ring (R^3, R^4) and substituents of the quinoline ring (R^5, R^6) as shown in Figure 3.

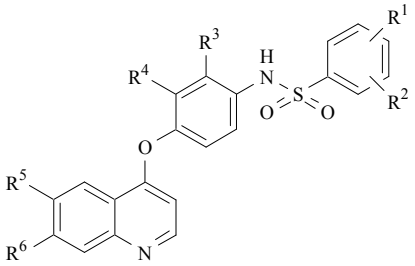

Figure 3. General structure of the prepared *N*-[4-(quinolin-4-yloxy)-phenyl]-benzenesulfonamide series

First, the effect of the benzenesulfonamide substituents (R^1, R^2) was evaluated as shown in Table 1, while the substituents of the quinoline and the *p*-aminophenol ring remained unchanged, identical to those in Ki8751 (**8**) (Figure 2). The analogous 2,4-difluoro derivative (**12h**) (IC_{50} = 6.400 μM) showed significantly weaker inhibitory potency against AXL than Ki8751 (**8**) (IC_{50} = 0.300 μM). However, we have discovered a number of compounds having submicromolar IC_{50}, from which 2-CF_3 (**12c**) and 2-OCF_3 (**12f**) groups showed the best results in this set (0.360 μM and 0.300 μM, respectively).

Table 1. Inhibitory activities of *N*-[4-(6,7-dimethoxy-quinolin-4-yloxy)-2-fluoro-phenyl]-benzenesulfonamide derivatives

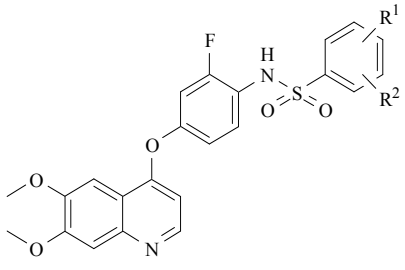

No	R^1	R^2	AXL $IC_{50}{}^a$ (μM)

12a	H	H	2.600
12b	2-CH_3	H	2.350
12c	2-CF_3	H	0.360
12d	3-CF_3	H	6.000
12e	2-OCH_3	H	>3.000
12f	2-OCF_3	H	0.300
12g	2-F	H	>1.000
12h	2-F	4-F	6.400
12i	2-F	5-F	0.840
12j	2-F	6-F	>1.000
12k	3-F	H	3.010
12l	2-Cl	H	>1.000
12m	2-Cl	5-Cl	1.610
12n	2-Cl	6-Cl	1.770
12o	3-Cl	4-F	>1.000

[a] IC_{50} values are average of at least two independent experiments

Optimization of substituents of the *p*-aminophenol ring revealed, that the R^3 and R^4 substituents (see Fig.3) can strongly influence the kinase inhibitory activity (Table 2.). Introducing a methyl group in either one of these positions (**12q**, **12r**) significantly reduced the AXL inhibitory effect. Surprisingly, in the case of methoxy and fluoro moieties we observed a diverse effect. In R^3 position these substituents did not cause considerable changes (**12s**, 0.289 μM; **12c**, 0.360 μM), however, in R^4 position the methoxy group reduced the effect (**12t**, 1.960 μM), while the fluorine substituent unexpectedly increased the AXL inhibitory effect (**12u**, 0.077 μM).

Table 2. Inhibitory activities of *N*-[4-(6,7-dimethoxy-quinolin-4-yloxy)-2-subtituted-phenyl]-2-trifluoromethyl-benzenesulfonamide derivatives

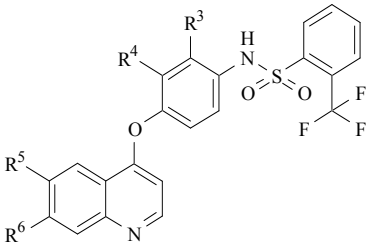

No.	R^3	R^4	AXL IC_{50}[a] (μM)
12p	H	H	0.350
12q	CH_3	H	>3.000
12r	H	CH_3	2.250
12s	CH_3O	H	0.289
12t	H	CH_3O	1.960
12c	F	H	0.360
12u	H	F	0.077

[a] IC_{50} values are average of at least two independent experiments

In the next step we explored the effect of R^5 and R^6 substituents and how interchangeable are they (Table 3). To evaluate the effect of bosutinib's (**2**) side chain, we introduced the 3-(4-methyl-piperazin-1-yl)-propoxy moiety into R^5 or R^6 position. We have discovered that compounds featuring this side chain in R^6 position (**18b**, **18d**) were significantly more potent than those in R^5 position (**18a**, **18c**). We have also found, that a methoxy substituent next to the 3-(4-methyl-piperazin-1-yl)-propoxy moiety (**18a** and **18c**; **18b** and **18d**) increased the inhibitory potency against AXL kinase. As a result, **18d** was identified as the most potent compound in this set with an IC_{50} of 0.021 μM.

Table 3. Inhibitory activities of *N*-(3-fluoro-4-{6,7-substituted-quinolin-4-yloxy}-phenyl)-2-trifluoromethyl-benzenesulfonamide derivatives

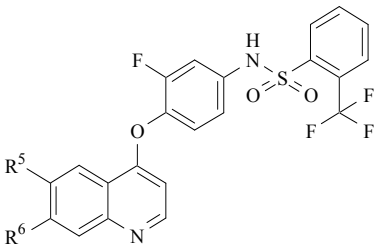

No.	R^5	R^6	AXL IC_{50}[a] (μM)
12u	CH_3O	CH_3O	0.077
18a	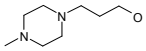	H	0.910
18b	H	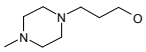	0.093
18c	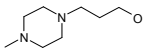	CH_3O	0.101
18d	CH_3O	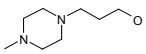	0.021

[a] IC_{50} values are average of at least two independent experiments

Having selected the optimal substituent combinations on the quinoline (R^5, R^6) and *p*-aminophenol ring (R^3, R^4), we aimed to re-evaluate the role of the R^1, R^2 substituents as shown in Table 4. Based on this comparison, in the group the 2-CF_3 moiety bearing (**18d**) remained to be the most active with 0.021 μM IC_{50}. Furthermore, the following substituents were confirmed to express similar efficacy against AXL kinase: 2-OCF_3 (**19e**), 2,5-diF (**19h**), 2,6-diF (**19i**).

Table 4. Inhibitory activities of *N*-(3-fluoro-4-{6-methoxy-7-[3-(4-methyl-piperazin-1-yl)-propoxy]-quinolin-4-yloxy}-phenyl)-benzenesulfonamide derivatives

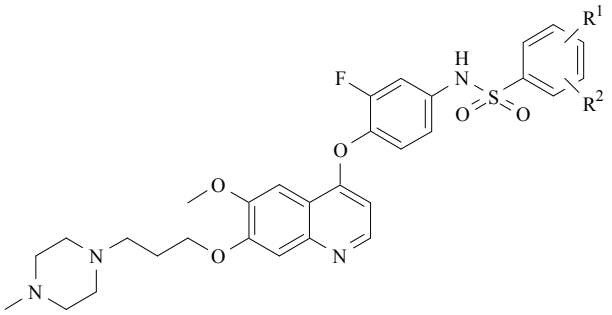

No.	R^1	R^2	AXL IC_{50}[a] (μM)
18d	2-CF_3	H	0.021
19a	H	H	0.218
19b	2-CH_3	H	0.430
19c	3-CF_3	H	0.354
19d	2-OCH_3	H	1.434
19e	2-OCF_3	H	0.051
19f	2-F	H	0.121
19g	2-F	4-F	0.380
19h	2-F	5-F	0.027
19i	2-F	6-F	0.035
19j	3-F	H	0.388
19k	2-Cl	H	0.184
19l	2-Cl	5-Cl	0.201
19m	2-Cl	6-Cl	0.068
19n	3-Cl	4-F	0.202

[a] IC_{50} values are average of at least two independent experiments

Finally, our attention was focused on the R^6 substituent. Two series of derivatives were prepared bearing 2-trifluoromethylbenzenesulfonamide (**18d**, **20a**-**20l**) or 2,5-

difluorobenzenesulfonamide (**19h**, **21a**-**21l**) moiety to validate the effect of the side chain. The results are summarized in Table 5 and Table 6. As a result of our optimization process we were able to identify numerous submicromolar AXL kinase inhibitors in this compound class.

Table 5. Inhibitory activities of *N*-(3-fluoro-4-{6-methoxy-quinolin-4-yloxy}-phenyl)-2-trifluoromethyl-benzenesulfonamide derivatives

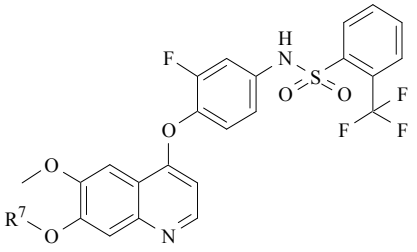

No.	R^7	AXL IC_{50}[a] (μM)
18d	3-(4-methyl-piperazin-1-yl)-propyl-	0.021
20a	2-(morpholin-4-yl)-ethyl-	0.054
20b	3-(morpholin-4-yl)-propyl-	0.021
20c	4-(morpholin-4-yl)-butyl-	0.021
20d	3-(piperidin-1-yl)-propyl-	0.018
20e	3-(2-methyl-piperidin-1-yl)-propyl-	0.070
20f	3-(3-methyl-piperidin-1-yl)-propyl-	0.031
20g	3-(4-methyl-piperidin-1-yl)-propyl-	0.046
20h	4-acetoxy-butyl-	0.046
20i	dimethylcarbamoylmethyl-	0.796
20j	3-(dimethylamino)-propyl-	0.027
20k	3-(tert-butoxycarbonylamino)-propyl-	0.170
20l*	3-amino-propyl-	0.238

[a] IC_{50} values are average of at least two independent experiments, *HCl salt

Table 6. Inhibitory activities of *N*-(3-fluoro-4-{6-methoxy-quinolin-4-yloxy}-phenyl)-2,5-difluoro-benzenesulfonamide derivatives

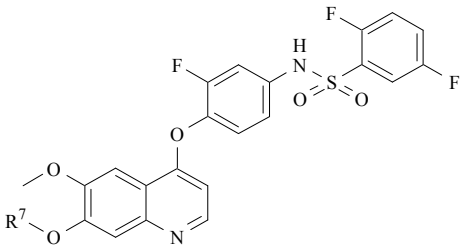

No.	R^7	AXL IC_{50}[a] (μM)
19h	3-(4-methyl-piperazin-1-yl)-propyl-	0.053
21a	2-(morpholin-4-yl)-ethyl-	0.052
21b	3-(morpholin-4-yl)-propyl-	0.035
21c	4-(morpholin-4-yl)-butyl-	0.027
21d	3-(piperidin-1-yl)-propyl-	0.072
21e	3-(2-methyl-piperidin-1-yl)-propyl-	0.050
21f	3-(3-methyl-piperidin-1-yl)-propyl-	0.028
21g	3-(4-methyl-piperidin-1-yl)-propyl-	0.016
21h	4-acetoxy-butyl-	0.091
21i	dimethylcarbamoylmethyl-	>1.000
21j	3-(dimethylamino)-propyl-	0.036
21k	3-(tert-butoxycarbonylamino)-propyl-	0.120
21l*	3-amino-propyl-	0.636

[a] IC_{50} values are average of at least two independent experiments, *HCl salt

A detailed protein-inhibitor co-crystal structure of AXL kinase has not been published yet. To identify the important pharmacophore features for the binding we used the Phase module of

Schrödinger Suite 2009 and determined a five point pharmacophore (AAAHR, survival score: 3.037) for the active molecules (Figure 4).

Site1	Site2	Distance (Å)
A2	A1	10.258
A2	A6	6.966
A2	H8	4.440
A2	R17	4.440
A1	A6	4.192
A1	H8	9.753
A1	R17	6.022
A6	H8	8.041
A6	R17	2.790
H8	R17	5.433

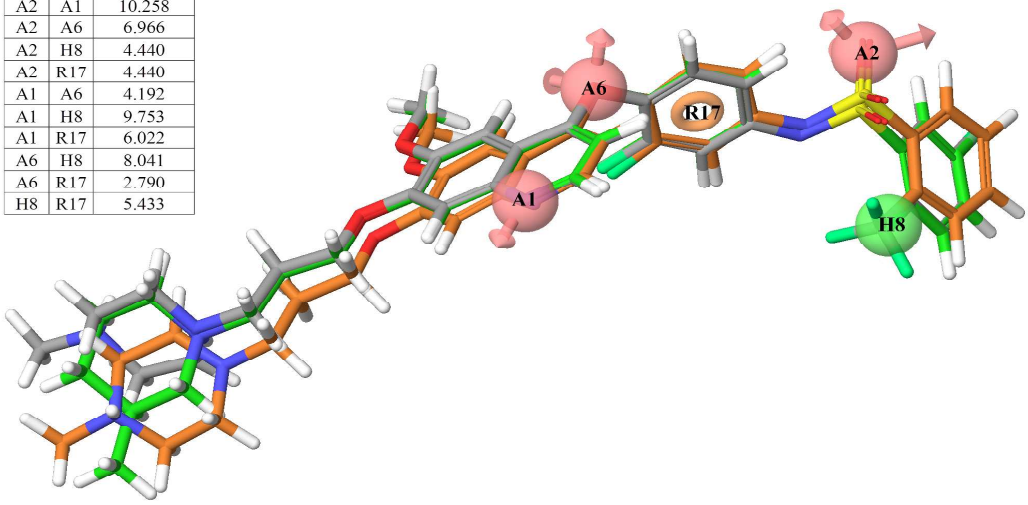

Figure 4. The five point pharmacophore of AXL kinase inhibitors. Compound **18d** (orange), **19h** (grey) and **21f** (green) are shown on the image.

The marked motifs (A1, A2, A6, H8, R17) are analogous in the best and the moderate active compounds, and according to other kinase inhibitors these points are necessary for the interactions with the hinge region (A1), DFG motif (A2) and gatekeeper residue (A2, R17). The *in vitro* AXL kinase assay revealed that the most active compounds differ in two motifs from less active ones. The flexible side chains in R^6 position enhance not only the inhibitory effect (Table 3) but the solubility as well. The position and substitution of the aromatic ring R17 is also crucial, because this phenyl ring can be involved in hydrophobic interactions with the gatekeeper residue (Leu620 of the AXL kinase). Although a small gatekeeper residue, like Leu620, could allow larger and more hydrophobic substituents, only small substituents are well tolerated, especially in R^3 and R^4 position (Table 2). Due to the size of the molecules the

whole large back cavity can be occupied by the sulfonamide group and the substituted phenyl ring.

Having identified the biochemical potency of our compounds against AXL kinase, cellular assays were performed. **18d**, **19e**, **19h**, **19i** and **21f**, all displaying low μM IC_{50} values of AXL phosphorylation, were selected for further characterization of kinase selectivity profiles and in migration and invasion related cell based assays.

First we determined the kinase selectivity profile of **18d**, **19h**, **19i** and **21f** using three different types of assays, namely IMAP, binding and HTRF assay. The kinase profile of **18d**, **19h**, **19i** and **21f** displayed common target profile by inhibition of AXL as well as c-MET, SRC, ABL, cKIT, TIE2, PDGFRbeta, AurA and VEGFR-2 with efficacy of 83-100% when used at 10 μM concentration (Figure 5). The comparison of the kinase selectivity profiles identified additional targets with lower affinity especially to compound **18d** such as DDR1, FLT3, RET, FGFR3, CSK, B-RAF, ERBB2, SYK, INSR, and JAK3. 50% of the tested kinases have not been targeted by any of the compounds with notable affinity.

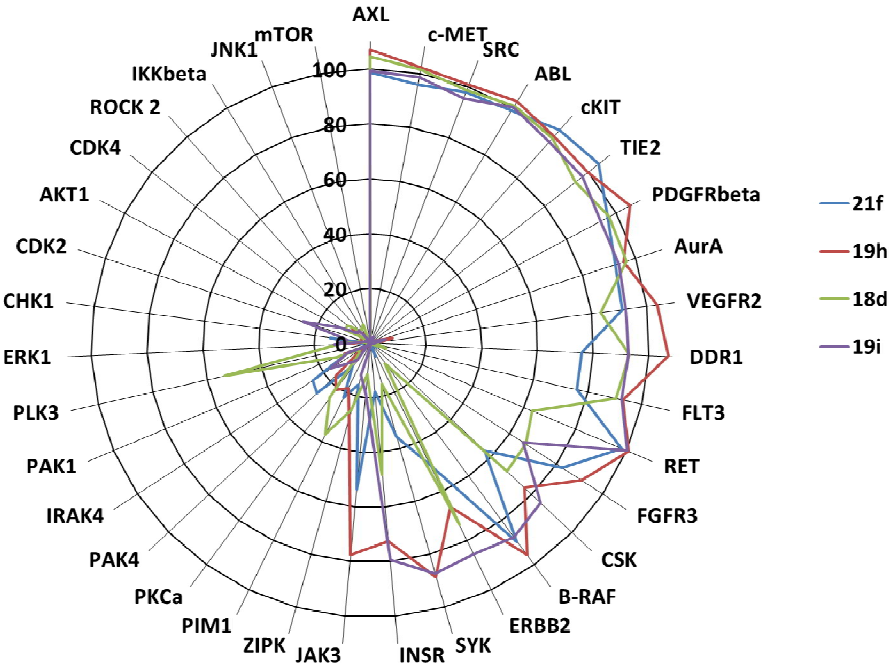

Figure 5. The kinase selectivity profile against a panel of 36 human kinases proves AXL as a common target of *N*-[4-(quinolin-4-yloxy)-phenyl]-benzenesulfonamides derivates. The selectivity profiling was performed in triplicates at a compound concentration of 10 μmol/L. The plots indicate the percentages of inhibition for each individual kinase.

We compared the molecular targets of N-[4-(quinolin-4-yloxy)-phenyl]-benzenesulfonamides derivates using the kinome-wide DiscoveRx KinomeScan assay. The kinase-binding selectivity of **20b** and **20g** was determined on a panel of 442 human wild type and mutated kinases (Kinomscan) (Supporting Information Table S1.). At 5 μmol/L, apart from the primary target AXL, 12 kinases (8 wild type kinases and 4 mutants) were identified as hits of **20b** and 23 of **20g** (17 wild type kinases and 6 mutants), exhibiting equal or lower percentage control values than of AXL (Supporting Information Table S2.). Lower numbers indicate stronger binding[20]. Additional common targets are ABL, LOK, cKIT, BRK, SRC, BLK, LCK, RIPK2, PDGFRA and B, CSF1R, c-MET, DDR1 and EGFR. ABL, cKIT; SRC; PDGFRbeta, c-MET and DDR1 were verified by chemical binding assays as displayed in Figure 5.

Increasing the threshold of percentage control to ten times the percentage control value of AXL we identified 45 out of 442 tested kinases for **20b** and 71 out of 442 for **20g** (Supporting Information Table S2.). This corresponds to 10.2% and 16.0% of the kinome being analyzed. Wilson et al, published the selectivity profiles of R428/BGB324 at a concentration of 1 μmol/L using a similar KinomeScan panel. This most selective AXL inhibitor published until now targets 24 kinases and mutants more potently than AXL and hits 128 out of 452 kinases and mutants within a range of ten times the percentage control value of AXL. This represents 27.8% of the tested kinome[20]. This data indicate a higher selectivity of N-[4-(quinolin-4-yloxy)-phenyl]-benzenesulfonamides **20b** and **20g** for AXL compared to R428/BGB324.

More in vivo relevant targets were analyzed by KinAffinity technology to determine the target profiles of the small molecule kinase inhibitors **19h** and **19i** in lysates from the human breast cancer cell line MDA-MB-231 (Table 7 and 8). The KinAffinity analysis of MDA-MB-231 lysates demonstrated a broad selectivity of compounds **19h** and **19i** for protein kinases. Target spectra for both compounds were fairly similar and revealed high affinities in the low nanomolar range for protein kinases AXL, c-MET, TNK1, MAP4K5, LYN, RIPK2, EGFR, SRC and several others.

The receptor tyrosine kinase AXL exhibited the highest affinity with a Kd value of 0.015 μM for compound **19h**. Additional target kinases with Kd values < 0.150 μM (10 fold the Kd of AXL) were TNK1, MAP4K5, LYN, c-MET, RIPK2, ACVR1, PLK4, FYN, AURKB, ABL2, EGFR and LIMK1. In summary, 13 protein kinases were identified with Kd values < 0.150 μM for compound **19h**. In total, 168 kinase targets were enriched from MDA-MB-231 cells, 48 of which were identified as target proteins of compound **19h** within a Kd range between 0.015 and 7.650 μM. This corresponds to 7.7% and 25% of the kinome being detected in MDA-MB231 cells. The remaining 126 kinases bound to the KinAffinity matrix but were not

competed by compound **19h**. Consequently, these kinases showed no binding characteristics expected for target proteins of compound **19h**. Table 7 shows the target protein kinases of compound **19h** in MDA-MB-231 cells. Targets were ranked according to their affinities and targets with low Kd values ranging from 0.015 to 7.650 μM.

Table 7. The target protein kinases of compound **19h** in MDA-MB-231 cells (analyzed by KinAffinity technology)

	Uniprot	**Protein Name**	**Gene Name**	**KD_free [μM]**
1	P30530	AXL oncogene	AXL	0.015
2	Q13470	Non-receptor tyrosine-protein kinase TNK1	TNK1	0.024
3	Q9Y4K4	Mitogen-activated protein kinase kinase kinase kinase 5	MAP4K5	0.024
4	P07948	Tyrosine-protein kinase Lyn	LYN	0.029
5	P08581	Tyrosine-protein kinase c-MET	c-MET	0.041
6	O43353	Receptor-interacting serine/threonine-protein kinase 2	RIPK2	0.043
7	Q04771	Activin receptor type I	ACVR1	0.052
8	O00444	Polo-like kinase 4	PLK4	0.053
9	P06241	Tyrosine-protein kinase Fyn	FYN	0.064
10	Q96GD4	Aurora kinase B	AURKB	>0.069
11	P42684	Tyrosine-protein kinase ABL2	ABL2	0.071
12	P00533	Epidermal growth factor receptor	EGFR	0.122
13	P53667	LIM domain kinase 1	LIMK1	0.130
14	P07947	Proto-oncogene tyrosine-protein kinase Yes	YES	0.178
15	P12931	Proto-oncogene tyrosine-protein kinase Src	SRC	0.254
16	P41240	Tyrosine-protein kinase CSK	CSK	0.270

17	Q14164	Inhibitor of nuclear factor kappa-B kinase subunit epsilon	IKKE	0.282
18	Q13131	5-AMP-activated protein kinase catalytic subunit alpha-1	PRKAA1	0.616
19	P16591	Tyrosine-protein kinase Fer	FER	0.679
20	O75460	Serine/threonine-protein kinase/endoribonuclease IRE1	IRE1	0.723
21	P54619	5-AMP-activated protein kinase subunit gamma-1	PRKAG1	0.825
22	O14965	Aurora kinase A	AURKA	0.847
23	O43741	5-AMP-activated protein kinase subunit beta-2	PRKAB2	0.969
24	Q9UGJ0	5-AMP-activated protein kinase subunit gamma-2	PRKAG2	1.078
25	Q9NYL2	Mitogen-activated protein kinase kinase kinase MLT	ZAK	1.180
26	Q9Y478	5-AMP-activated protein kinase subunit beta-1	PRKAB1	1.257
27	P37173	Transforming growth factor-beta receptor type II	TGFBR2	1.860
28	Q8IVH8	Mitogen-activated protein kinase kinase kinase kinase 3	MAP4K3	2.080
29	Q13043	Mammalian STE20-like protein kinase 1	MST1	2.433
30	O14976	Cyclin-G-associated kinase	GAK	2.448
31	Q6PHR2	Serine/threonine-protein kinase ULK3	ULK3	>2.514
32	Q13011	Delta(3,5)-Delta(2,4)-dienoyl-CoA isomerase	ECH1	2.857
33	Q99759	Mitogen-activated protein kinase kinase kinase 3	MAP3K3	3.133
34	Q15418	90 kDa ribosomal protein S6 kinase 1	RPS6KA1	3.152
35	Q92844	TRAF family member-associated NF-kappa-B activator	TANK	3.418
36	O95819	Mitogen-activated protein kinase kinase kinase kinase 4	MAP4K4	3.75
37	O94804	Lymphocyte-oriented kinase	LOK	3.78
38	P27448	MAP/microtubule affinity-regulating kinase 3	MARK3	3.854
39	Q9Y2U5	Mitogen-activated protein kinase kinase kinase 2	MAP3K2	4.396
40	Q05397	Focal adhesion kinase 1	FAK	4.445
41	Q7KZI7	MAP/microtubule affinity-regulating kinase 2	MARK2	4.455

42	Q9H0K1	Qin-induced kinase	QIK	4.518
43	Q96PY6	Never in mitosis A-related kinase 1	NEK1	5.146
44	Q96L34	MAP/microtubule affinity-regulating kinase 4	MARK4	5.975
45	Q07002	Serine/threonine-protein kinase PCTAIRE-3	PCTK3	>6.194
46	Q13188	Mammalian STE20-like protein kinase 2	MST2	>6.454
47	P36507	Dual specificity mitogen-activated protein kinase kinase 2	MAP2K2	6.917
48	Q00537	Serine/threonine-protein kinase PCTAIRE-2	PCTK2	>7.651

The receptor tyrosine kinase AXL and the receptor tyrosine-protein kinase c-MET exhibited the highest affinities each with a Kd value of 0.006 μM for compound **19i**. Additional high affinity target kinases with Kd values < 0.060 μM (10 fold the Kd of AXL) were MAP4K5, LYN, TNK1, ABL2, EGFR, RIPK2, CSK, FYN, YES, and PLK4. In summary, 13 protein kinases were identified with Kd values < 0.060 μM for compound **19i**. In total, 168 kinase targets were enriched from MDA-MB-231 cells, 52 of which were identified as target proteins of compound **19i** within a Kd range between 0.006 and 9.230 μM. This corresponds to 7.7% and 25.6% of the kinome being detected in MDA-MB231 cells. The remaining 125 kinases bound to the KinAffinity matrix but were not competed by compound **19i**. Consequently, these kinases showed no binding characteristics expected for target proteins of compound **19i**. Table 8 shows the target protein kinases of compound **19i** in MDA-MB-231 cells. Targets are ranked according to their affinities with Kd values ranging from 0.006 to 9.230 μM.

Table 8. The target protein kinases of compound **19i** in MDA-MB-231 cells (analyzed by KinAffinity technology)

Uniprot	**Protein Name**	**Gene**	**KD_free**

			Name	[μM]
1	P30530	AXL oncogene	AXL	0.006
2	P08581	Tyrosine-protein kinase c-Met	MET	0.006
3	Q9Y4K4	Mitogen-activated protein kinase kinase kinase kinase 5	MAP4K5	0.008
4	P07948	Tyrosine-protein kinase Lyn	LYN	0.011
5	Q13470	Non-receptor tyrosine-protein kinase TNK1	TNK1	0.014
6	P42684	Tyrosine-protein kinase ABL2	ABL2	0.016
7	P00533	Epidermal growth factor receptor	EGFR	0.016
8	O43353	Receptor-interacting serine/threonine-protein kinase 2	RIPK2	0.017
9	P41240	Tyrosine-protein kinase CSK	CSK	0.030
10	Q96GD4	Aurora kinase B	AURKB	0.034
11	P06241	Tyrosine-protein kinase Fyn	FYN	0.038
12	P07947	Proto-oncogene tyrosine-protein kinase Yes	YES	0.040
13	O00444	Polo-like kinase 4	PLK4	0.048
14	Q04771	Activin receptor type I	ACVR1	>0.070
15	P53667	LIM domain kinase 1	LIMK1	0.093
16	P12931	Proto-oncogene tyrosine-protein kinase Src	SRC	0.096
17	Q14164	Inhibitor of nuclear factor kappa-B kinase subunit epsilon	IKKE	0.122
18	O14965	Aurora kinase A	AURKA	0.146
19	P36897	Transforming growth factor-beta receptor type I	TGFBR1	0.205
20	O75460	Serine/threonine-protein kinase/endoribonuclease IRE1	IRE1	0.243
21	P16591	Tyrosine-protein kinase Fer	FER	0.304
22	Q13163	Dual specificity mitogen-activated protein kinase kinase 5	MAP2K5	0.539
23	Q13131	5-AMP-activated protein kinase catalytic subunit alpha-1	PRKAA1	0.786
24	Q8IVH8	Mitogen-activated protein kinase kinase kinase kinase 3	MAP4K3	1.367

25	Q92844	TRAF-interacting protein	TANK	1.567
26	P54619	5-AMP-activated protein kinase subunit gamma-1	PRKAG1	1.871
27	O43741	5-AMP-activated protein kinase subunit beta-2	PRKAB2	1.907
28	Q13043	Mammalian STE20-like protein kinase 1	MST1	2.080
29	TBKBP1	TANK-binding kinase 1-binding protein 1	TBKBP1	2.090
30	Q05397	Focal adhesion kinase 1	FAK	2.212
31	Q9Y478	5-AMP-activated protein kinase subunit beta-1	PRKAB1	2.279
32	Q9UGJ0	5-AMP-activated protein kinase subunit gamma-2	PRKAG2	2.296
33	Q6PHR2	Serine/threonine-protein kinase ULK3	ULK3	>2.513
34	P53671	LIM domain kinase 2	LIMK2	2.784
35	Q9H6S1	5-azacytidine-induced protein 2	AZI2	2.982
36	O94804	Lymphocyte-oriented kinase	LOK	3.039
37	Q9NYL2	Mitogen-activated protein kinase kinase kinase MLT	ZAK	3.210
38	Q9UHD2	TANK-binding kinase 1	TBK1	3.273
39	Q9H0K1	Qin-induced kinase SNF1-like kinase 2	QIK	3.545
40	P42680	Tyrosine-protein kinase Tec	TEC	>3.674
41	O14976	Cyclin-G-associated kinase	GAK	4.166
42	Q96PY6	Never in mitosis A-related kinase 1	NEK1	5.043
43	Q13188	Mammalian STE20-like protein kinase 2	MST2	5.223
44	Q15418	90 kDa ribosomal protein S6 kinase 1	RPS6KA1	5.474
45	Q9Y2U5	Mitogen-activated protein kinase kinase kinase 2	MAP3K2	5.518
46	P27448	MAP/microtubule affinity-regulating kinase 3	MARK3	5.622
47	Q14289	Focal adhesion kinase 2	PYK2	6.928
48	Q7KZI7	MAP/microtubule affinity-regulating kinase 2;	MARK2	7.086
49	P37173	Transforming growth factor-beta receptor type II	TGFBR2	7.385

50	Q9Y2K2	Serine/threonine-protein kinase QSK	QSK	7.630
51	P36507	Dual specificity mitogen-activated protein kinase kinase 2	MAP2K2	8.852
52	P30084	Enoyl-CoA hydratase 1	ECHS1	9.237

Complete lists of all kinases that bound to the KinAffinity matrix and of all identified target kinases of compound **19h** and **19i** are provided in Supporting Information Table S3. This gave us the opportunity to discriminate between *N*-[4-(quinolin-4-yloxy)-phenyl]-benzenesulfonamides derivates with higher and lower target selectivity profiles to AXL.

To elucidate the affinities of examples **18d**, **19e**, **19h**, **19i, 20b, 20g** and **21f** to four migration related kinases in more detail, we determined IC_{50} values for AXL, SRC, c-MET and EGFR kinases (Table 9). All seven examples exhibit low IC_{50} values for AXL confirming the high affinity of these *N*-[4-(quinolin-4-yloxy)-phenyl]-benzenesulfonamides as AXL inhibitors. The affinity to SRC, c-MET and EGFR was more variable for the tested examples. (Table 9.) The IC_{50} values especially for c-MET and EGFR were increasing from 0.127 μM for c-MET and 0.178 μM for EGFR using example **19i,** to 1.535 μM for c-MET and 3.081 μM for EGFR in the case of example **19e**. The IC_{50} values were increasing in general from **19i** < **19h** <**18d** < **20b** < **20g** < **21f** < **19e** identifying **19e** as the most selective compound for AXL. Finally we were able to categorize compound **19i** and **19h** into a lower selective group, **18d**, **20b**, **20g** as an intermediate group and **21f** and **19e** as compounds with higher selectivity for AXL.

Table 9. The IC_{50} values of *N*-[4-(quinolin-4-yloxy)-phenyl]-benzenesulfonamide derivates on AXL, SRC, c-MET and wild type EGFR. The IC_{50} determinations were performed in triplicates.

No.	AXL IC_{50} (μM)	SRC IC_{50} (μM)	c-MET IC_{50} (μM)	EGFR wt IC_{50} (μM)
19i	0.035	0.044	0.127	0.178
19h	0.027	0.088	0.358	0.149

18d	0.021	0.544	0.488	0.281
20b	0.021	0.995	0.338	0.650
20g	0.027	1.723	0.609	0.592
21f	0.028	0.113	1.307	1.128
19e	0.051	1.951	1.535	3.081

Overexpression of the RTK AXL and its implication in the migration and invasion of mammary carcinoma has already been demonstrated in various publications.[21, 22] Therefore we studied the impact of *N*-[4-(quinolin-4-yloxy)-phenyl]-benzenesulfonamides derivates on AXL mediated migration and invasion of an AXL-overexpressing human breast cancer cell line, namely MDA-MB231.

First, we determined the inhibitory effect of **18d**, **19e**, **19h**, **19i** and **21f** on cell migration using Boyden chamber assays. The IC_{50} value was 1.5 µM for **19i**, 2.5 µM for **19h**, 3.3 for **21f**, 4.6 µM for **18d** and 4.3 µM for **19e** in MDA-MB231 cells (Figure 6 and 7).

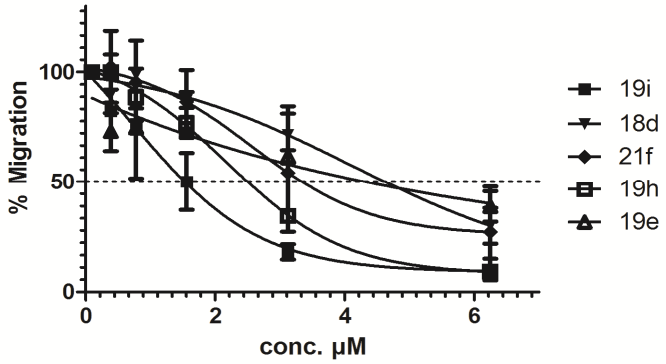

Figure 6. Migration inhibition (%) of the compounds

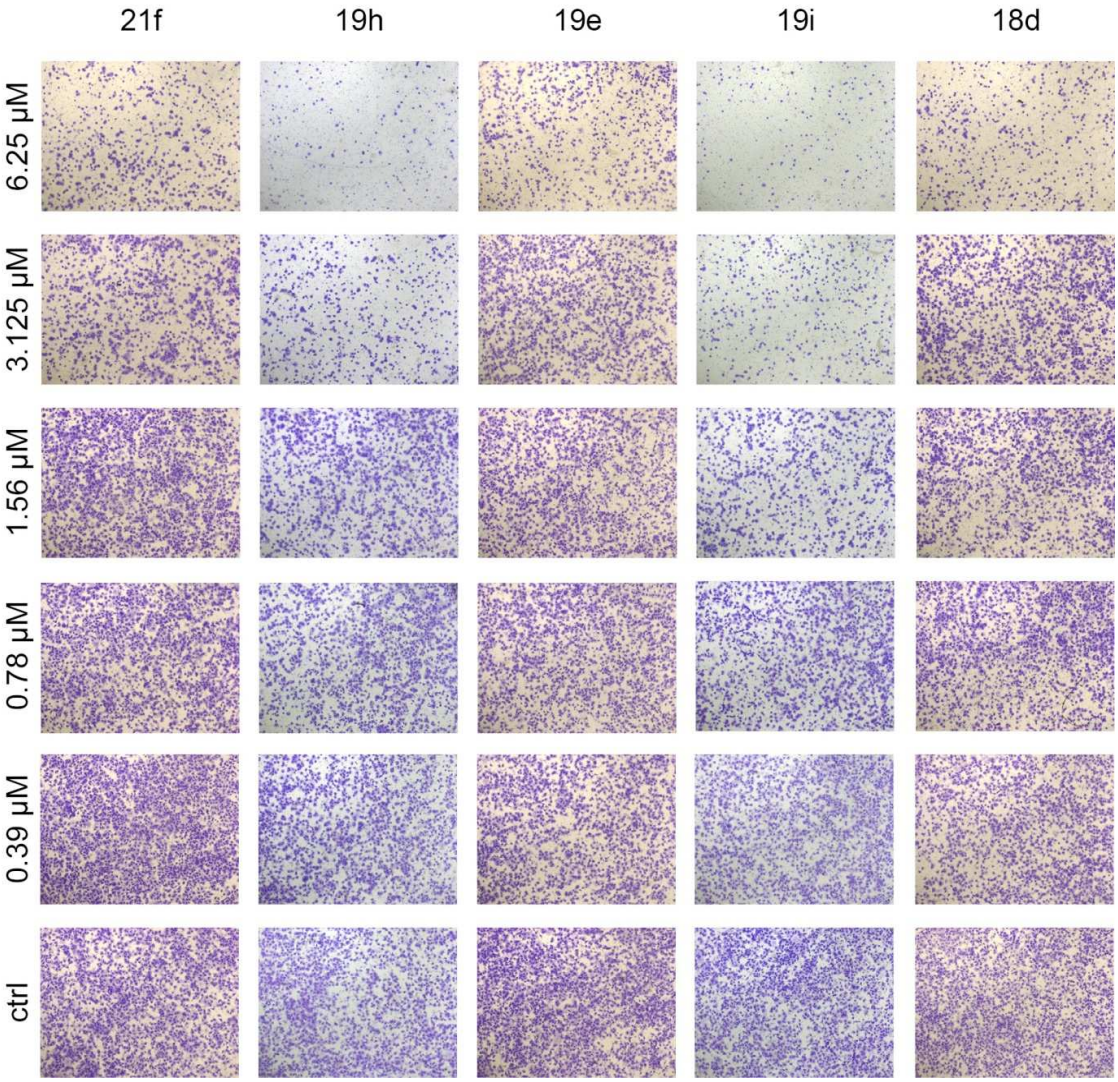

Figure 7. Representative images of MDA-MB231 trans-migrating the porous membrane. MDA-MB231 cells were incubated with indicated compound concentrations relative to DMSO control for 3.5 hours. Scale bars indicate 100 µm.

Comparing the IC_{50} values we discovered that migration inhibition was correlating with the selectivity profiles of the compounds. Thereby it was evident that less selective compounds, namely **19h** and **19i**, were superior in blocking migration of MDA-MB-231 cells in contrast to more AXL selective derivates, in terms of migration related kinases, like SRC, c-MET and EGFR as displayed in Table 9. A similar conclusion were drawn by Pénzes et al, 2014, that inhibition of MDA-MB231 cell migration by AXL inhibitors is dependent on additional

targets like a SRC family kinase LYN and the migration related CRK-associated substrate p130Cas[23].

In summary, the inhibition values of migration were significantly (more than 50-fold) higher than those determined for inhibition of AXL phosphorylation, suggesting that migration of MDA-MB231 does not solely depend on AXL phosphorylation, but might be regulated by multiple additional kinases such as SRC, c-MET and EGFR.

Secondly, we determined the inhibitory effect of **18d**, **19e**, **19h**, **19i** and **21f** on invasion of MDA-MB231 cells (Figure 8). MDA-MB231 cell have the ability for invasion of semisolid Matrigel. We used this capacity of MDA-MB231 cells and seeded a single cell suspension on top of a solid Matrigel. Then we allowed the single cells to migrate towards each other within 5 hours, resulting in the formation of large cell aggregates (Figure 9). Compounds blocking invasion are able to arrest MDA-MB231 cells in a single cell status prohibiting mesenchymal cell invasion and subsequent aggregate formation. The percentage of the large multicellular aggregates was subsequently quantified.

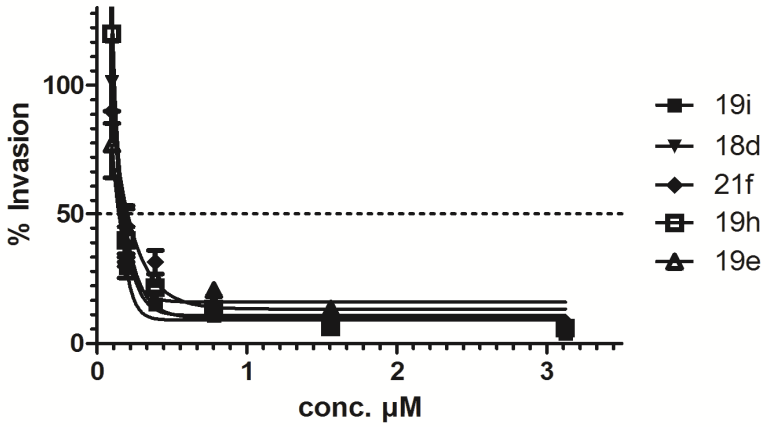

Figure 8. Invasion inhibition (%) of the molecules

The IC_{50} value for aggregate formation was 156 nM for **19i**, 158 nM for **19h**, 185 nM for **21f**, 158 nM for **18d** and 103 nM for **19e** in MDA-MB231 cells. The comparison of IC_{50} values of invasion and aggregate formation correlated with the IC_{50} values of AXL phosphorylation inhibition. Thereby it was evident that all compounds exhibit very similar IC_{50} blocking invasion of MDA-MB-231 cells in nM range.

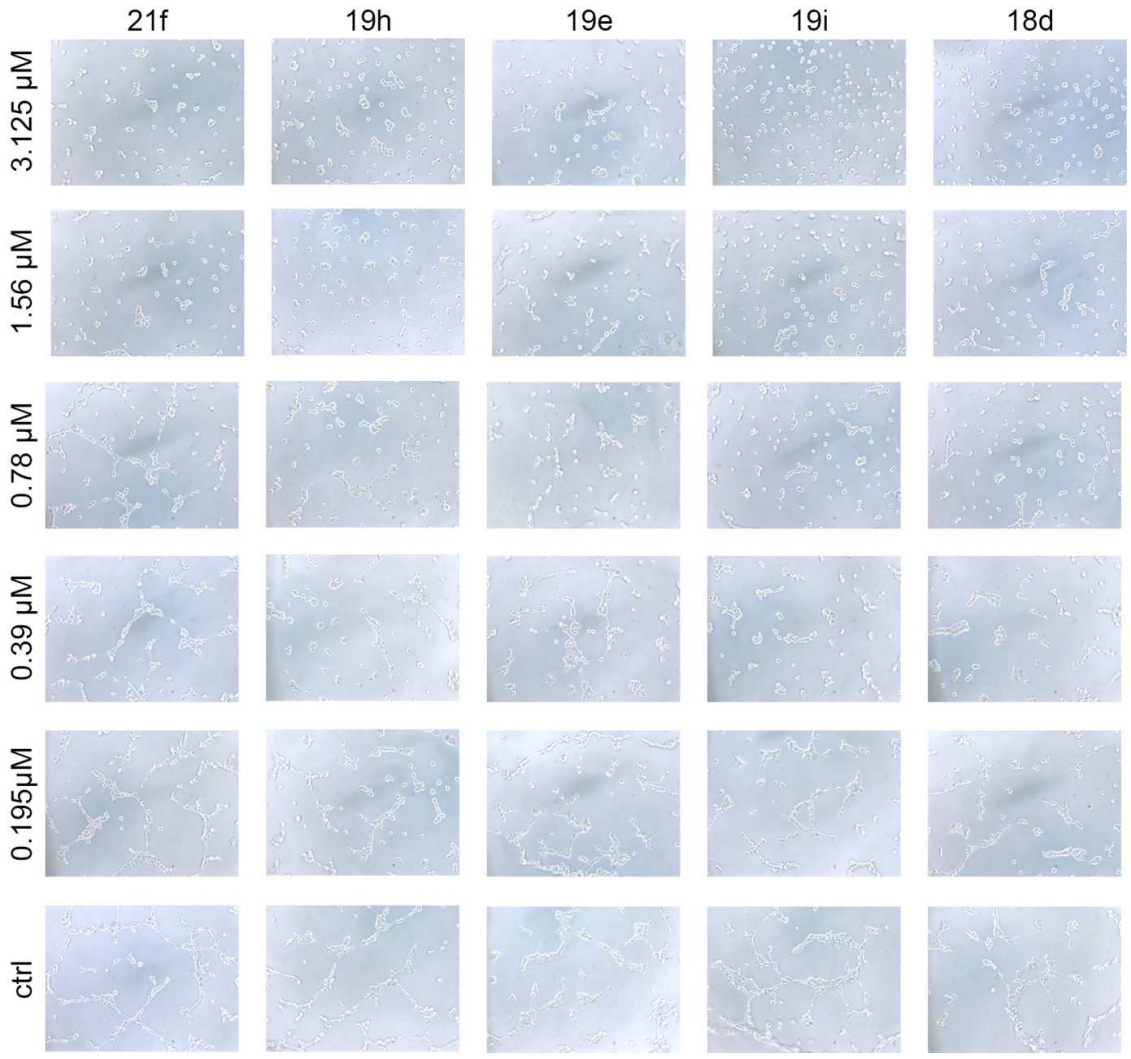

Figure 9. Representative images of MDA-MB231 aggregates. MDA-MB231 cells were incubated with indicated compound concentrations relative to DMSO control for 5 hours. Scale bars indicate 100 µm.

In summary, the inhibition values of invasion were two- to six-fold higher than those determined for inhibition of AXL phosphorylation, suggesting that invasion inhibition of MDA-MB231 is closely correlated to AXL phosphorylation inhibition in contrast to migration. This is in line with the results that invasion is more affected than migration by AXL specific siRNA in colorectal cancer cell lines[24], AXL specific blocking antibody 20G7-D9 in triple-negative breast cancer cell line HBL-100[25] and selective RNA-based aptamer, GL21.T that binds the extracellular domain of AXL at high affinityAXL specific Aptamer in GBM cell line U87MG[26].

Migration inhibition correlates positively with lower selectivity of *N*-[4-(quinolin-4-yloxy)-phenyl]-benzenesulfonamides towards AXL kinase and highlights the importance of additional migration related kinases, as EGFR, c-MET, SRC family kinases, LIMK1 or ABL. These migration related kinases were validated as target proteins with < 1µM Kd-values in MDA-MB231 cells using KinAffinity. Nevertheless, we cannot exclude other factors being important for metastasis inhibition as shown for NK-cell activation in vivo[27].

Two compounds **19h** and **21f** exhibiting good selectivity profiles and low nanomolar AXL inhibition values were selected for further ADME and pharmacokinetic studies. The obtained parameters for compound **19h** and **21f** are summarized in Table 10.

Table 10. ADME and pharmacokinetic parameters obtained for compound **19h** and **21f**

Parameter	**19h**	**21f**
SolRank pH 7.4 rel. Conc. [µM]	68.8	18.0
PAMPA pH 7.4 %Flux [%]	24.3	46.1
Caco-2 P_{app} A->B [10^{-6} cm/s]	7.4	2.4

Caco-2 P_{app} B->A [10^{-6} cm/s]	17.0	14.6
Caco-2 RatioB->A:A->B	2.3	6.6
Microsomal Stab. Phase I human Clint [µL/min/mg]	60.5	18.3
Microsomal Stab. Phase I murine Clint [µL/min/mg]	143.3	19.1
Plasma Stab. Human %Remain	96.3	99.1
Plasma Stab. Murine %Remain	108.0	98.8
Plasma Protein Binding human %Bound	99.1	98.5
Plasma Protein Binding murine %Bound	97.2	95.9
PK mouse IV AUC(0-INF) [ng*h/mL]	2646.0	1395.0
PK mouse IV AUC(0-Tz) [ng*h/mL]	1433.0	669.0
PK mouse IV CL [l/h/kg]	0.4	0.7
PK mouse IV C0 [ng/mL]	310.0	216.0
PK mouse IV $t_{1/2}z$ [h]	18.7	8.5
PK mouse IV Vz [l/kg]	10.2	8.8

Compound **21f** and **19h** displayed a good solubility at pH 7.4 (18.0 or 68.8 µM, respectively) and exhibited a good permeability in PAMPA and Caco-2 assays. The intrinsic clearance had been assessed by microsomal stability assays displaying sufficient stability of 18.3 µL/min/mg in human microsomes and 19.1 µL/min/mg in mouse microsomes for compound **21f**, and 60.5 µL/min/mg in human microsomes and 143.3 µL/min/mg in mouse microsomes for compound **19h**. Both compounds feature very high human and murine plasma stability and are characterized by low plasma protein binding especially to murine plasma proteins with 95.9% and 97.2 % (Table 10).

After intravenous (iv) administration (3 mg/kg), compound **21f** demonstrated a good volume of distribution (Vz) of 8.8 l/kg in mouse and low systemic clearance (Cl) of 0.7 l/h/kg and a favorable half life ($t_{1/2}$) of 8.5 hours. Compound **19h** was characterized by slightly better volume of distribution (Vz) of 10.2 l/kg in mouse and lower systemic clearance (Cl) of 0.4 l/h/kg and a good half life ($t_{1/2}$) of 18.7 hours. Both compounds were well tolerated after oral administration (300 mg/kg), but unfortunately the measured oral bioavailability was very poor in mice.

On the basis of its encouraging pharmacokinetic profile, compound **21f** was evaluated in *in vivo* efficacy studies (Figure 10).

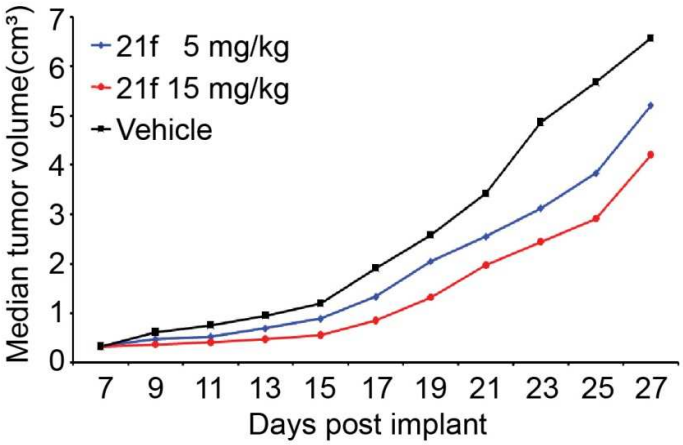

Figure 10. Tumor volume reduction of compound **21f**

An AXL expressing MXT mammary tumor xenograft model was examined in which tumor cells were implanted subcutaneously and staged to approximately 125 mm^3 prior to commencement of daily intraperitoneal (ip) dosing of the compound for 21 consecutive days. Compound **21f** was active at all dose levels tested as defined by >50% tumor growth inhibition (TGI) over one tumor volume doubling time (TVDT). The minimum efficacious dose of 5 mg/kg corresponded with prolongation of survival time to 118%. (Table 11).

Table 11. *In vivo* efficiency of compound **21f**

	Dose (mg/kg)	Treatment	Adm.	Animal	Survival (days)	Average ± SD	T/Cx
Vehicle	-	21 x qd	ip	7	30, 30, 31, 31, 32, 32, 33	31,28 ± 1,11	100%
21f	5	21 x qd	ip	7	35, 35, 36, 37, 37, 39, 39	36,86 ± 1,68	118%
21f	15	21 x qd	ip	7	36, 37, 39, 39, 42, 43, 43	39,86 ± 2,85	127%

The antitumor activity of example **21f** was dose responsive, and the compound reduced the tumor size by 40% compared to vehicle treatment after 3 weeks at a dose of 15 mg/kg and simultaneously prolonged the average survival time of the animals by 27% (Table 11). No overt toxicity was observed at any of these dose levels as defined by weight loss or morbidity.

Subsequently we performed a study to determine anti-metastatic efficacy of **19h** against the MDA-MB231 human breast tumor in female SCID/Beige mice, as reference treatment, paclitaxel was included for comparison. The mice were inoculated with MDA-MB-231 human breast tumor cells, orthotopically into the third mammary fat pad. Mice received treatment with either vehicle control, **19h** (30 mg/kg) or paclitaxel (10 mg/kg). vehicle control and **19h** were administered twice daily via intraperitoneal injection. paclitaxel was administered three times weekly via intravenous injection.

Body weight and tumor size measurements were made three times weekly for the duration of the study. Overall, there was significant mean body weight gain over the course of the study in the groups treated with vehicle control, **19h** and paclitaxel (Figure 11).

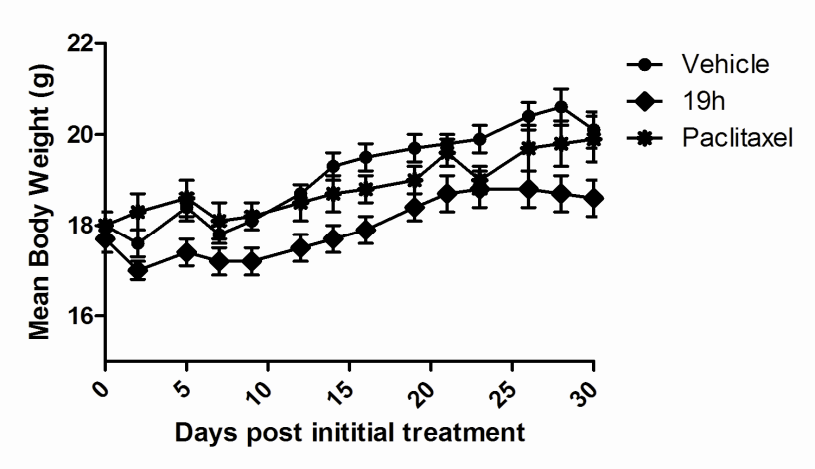

Figure 11. Average Body Weight of female SCID/Beige mice

In contrast to **19h** tumor growth was dramatically inhibited by paclitaxel (Figure 12).

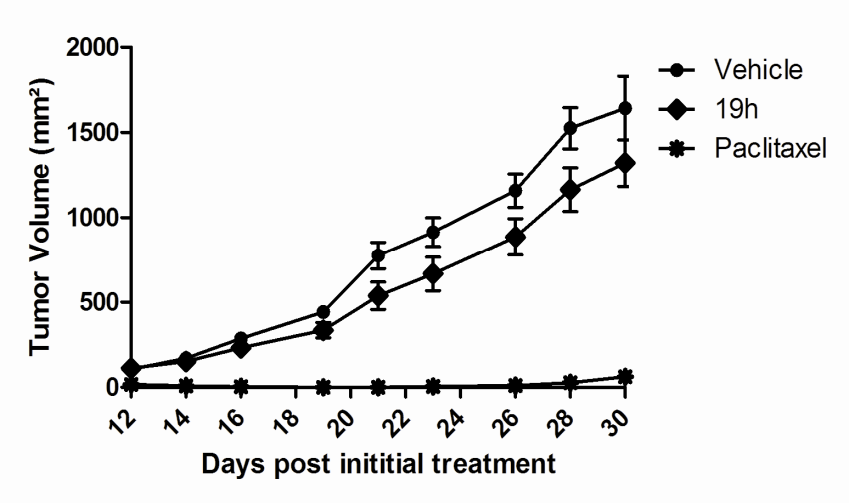

Figure 12. Growth of MDA-MB-231 tumor

Lung surface metastases and lymph node metastasis were assessed after formalin fixation, embedding, sectioning and H&E for assessment of tumor cell infiltration. Although treatment with **19h** was not efficacious in inhibiting growth of the primary tumors, lung metastases were reduced by 65.7% and lymph node infiltrates by 14.3% compared with the vehicle control. The reference control treatment, paclitaxel, resulted in 54.3% inhibition of total lung metastases compared with vehicle control, but did not prevent tumor cell infiltration into the regional lymph nodes compared with vehicle control as displayed in Figures 13 and 14.

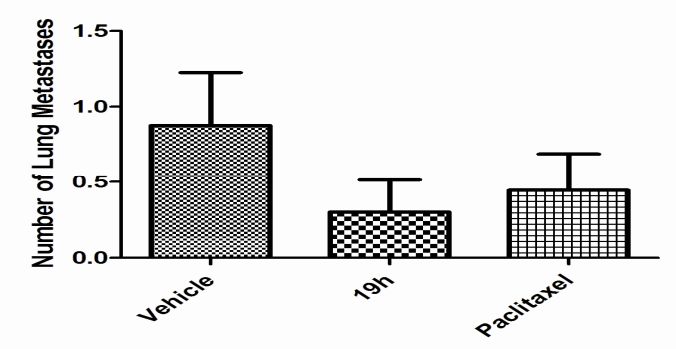

Figure 13. Mean Total Number of Lung Surface Metastases

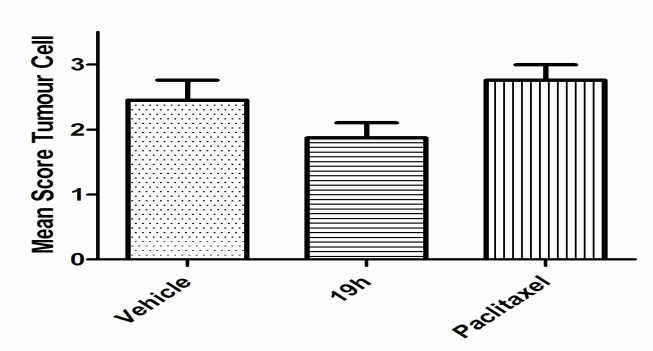

Figure 14. Mean Score for Tumour Cell Infiltration in Lymph Nodes

CONCLUSIONS

In conclusion, novel substituted *N*-[4-(quinolin-4-yloxy)-phenyl]-benzenesulfonamides were identified as potent inhibitors of AXL kinase. Optimization of the series SARs led to the identification of example **21f**, as a selective and applicable AXL kinase inhibitor. A partial tumor stasis of 40% tumor growth was achieved in the MXT human mammary carcinoma xenograft model following ip administration with no observed toxicity.

On the basis of its favorable *in vivo* efficacy, pharmacokinetic profile, and safety profile, **19h** was additionally used to determine anti-metastatic activity in an orthotopic and metastatic breast cancer model using human MDA-MB231 cell. Thereby we could prove the selective inhibition of lung surface metastasis by **19h** by 65.7% compared to vehicle control.

EXPERIMENTAL SECTION

General information

The commercially available reagents and solvents were used without further purification. The reactions were monitored by TLC, with Kieselgel 60 F_{254} (Merck) plates and visualized by UV light. Analytical data of compounds can be found in the Supporting Information. Analytical HPLC-MS was performed on a Waters HPLC-MS system using reverse phase. Method A: Waters XBridge C18 (5 cm x 4.6 mm, 5 μm), gradient 0-95 % B (0.00 min 5 % B, 0.50 min 5 % B, 5.50 min 95 % B, 6.00 min 95 % B, 6.50 min 5 % B, 7.00 min 5 % B), Solvent A: Water/ 0.05% HCO_2H, Solvent B: AcCN/ 0.05% HCO_2H over 7.00 min, flow = 2.0 mL/min. Separation module was Waters Alliance 2795. Method B: Waters X Waters XBridge C18 (5 cm x 4.6 mm, 3.5 μm), gradient 0-95 % B (0.00 min 5 % B, 0.50 min 5 % B, 5.5 min 95 % B, 6.00 min 95 % B, 6.50 min 5 % B, 7.00 min 5 % B), Solvent A: 5 mM NH_4HCO_3, Solvent B: AcCN over 7.00 min, flow = 2.0 mL/min. The separation module was Waters Alliance 2795. UV spectra were recorded using a Waters 996 DAD UV detector. Mass spectra were obtained using Waters SQD MS detector (ionization: ES^+/ES^-, source block temp: 120 °C, desolvation temp: 350 °C, desolvation gas: 400 L/h, cone gas: 100 L/h, capillary: 3000 V, cone: 25 V, extractor: 3 V, Rf lens: 0.2 V, scan: 120 to 1000 m/z in 1 sec., inter-scan delay: 0.1 s). The NMR spectra were recorded on a Bruker Avance 300 MHz AV spectrometer operating at 7.05 Tesla magnetic field, equipped with a 5 mm dual invese *z*-grad probehead, in deuterated dimethylsulfoxide (DMSO-d_6) solution, at 30 °C. The instrument was controlled and the data were processed using TopSpin 1.3 software package. Chemical shifts (δ) are in parts per million (ppm) referenced to tetramethylsilane. HRMS was performed on an Agilent 6230C TOF LC/MS System with Agilent Jet Stream source, ESI positive mode. Buffer: ammonium-formate in water / acetonitrile. Drying gas: 325 °C. V Cap: 3000 V. Fragmentor 100 V. Melting points were determined on a Büchi Melting Point B-540

instrument. All final compounds were purified to have ≥95% purity, controlled by analytical HPLC/UV/MS method (as described above) and confirmed by NMR.

Synthesis of compounds

The detailed synthesis procedures of the compounds, the purity and the chemical structure characterization are described in the Supporting Information.

Molecular modeling

The molecular modeling and pharmacophore model generation was carried out by Schrödinger Suite 2009 update 2 with the Confgen, LigPrep, Maestro and Phase programs. The 3D structures of the molecules were generated by the LigPrep v2.3 on pH = 7.4 using the OPLS_2005 force field. All conformers were produced by Confgen with default settings. To specify the common pharmacophore features of the inhibitors we applied Phase v3.1 which utilized a set of six pharmacophore points for model generation. These features were: H-bond acceptor (A), H-bond donor (D), hydrophobic group (H), negatively (N) and positively ionizable (P) and aromatic ring (R). After the site creations pharmacophore hypotheses were generated, scored and ranked by the software.

Biological assays

Cellular assays

MDA-MB231 cells were grown in Dulbecco's modified Eagle's medium supplemented with 1% sodium pyruvate (GE Heathcare, Wien, Austria), supplemented with 1% glutamine (GE Heathcare, Wien, Austria). Media were purchased from GIBCO and supplemented with 10% fetal calf serum (GIBCO, Invitrogen, Bleiswijk, Netherlands). Cells were maintained at 37°C in a humidified atmosphere containing 5% CO_2.

3D spheroid culture

BD Matrigel™ Matrix Basement membrane (BD Bioscience, USA, #354234) was diluted at a concentration of 3 mg/mL in cell line corresponding serum free medium. 80 µL of pre-cooled Matrigel was pipetted into the wells of pre-cooled 96-well plates. The Matrigel polymerized at least 16 hours at 37°C. 7000 cells/well in 120 µL of medium were seeded on top of the solid Matrigel and formed aggregates 5 hours. Inhibitor treatments were initiated at the moment of cell seeding into Matrigel.

Cell migration assay

The motility of the cells was determined by modified Boyden chamber assay. Cells were plated in medium with 0.1% FCS and transmigrated a 8 µm pores membrane(BD Transduction Laboratories, Heidelberg, Germany) towards medium with 1% FCS serving as a chemoattractant for 3.5h. The cells which had traversed the membrane were counted on images taken with Axiovert 300 Microscope (Zeiss, Jena, Germany). At least 5 random fields were counted per well.

Phospho-AXL ELISA

AXL phosphorylation was determined using phosphotyrosine AXL enzyme-linked immunosorbant assay (p-Tyr-AXL ELISA). 75000 NIH/3T3-AXL cells were seeded onto 6-well plates, starved for 24 hours and then treated with serially diluted inhibitor concentrations for 1 hour. Cells were lysed on ice in 400 µL lysis buffer for 15 minutes. 96-well Nunc MicroWell™ plates (Fisher Scientific GmbH, Germany) were coated overnight with 2 µg/mL of homemade anti-AXL capture antibody (homemade clone 259/2, IgG1 isotype) in PBS (100 µL/well). Subsequently 96-well plates were blocked with PBS/0.05% Tween®20 (Sigma-

Aldrich, Germany) + 10% FBS for 4 hours at 37 °C. Plates were washed 5 times with PBS/0.05% Tween®20 and 95 µL of lysate was transferred per well for incubation overnight at 4 °C. Plates were washed 5 times with PBS/0.05% Tween®20. For detection of phosphorylated tyrosine we used the biotinylated homemade anti-p-Tyr clone 4G10 antibody (0.5 µg/mL) in PBS/0.05% Tween®20 + 10% FBS (100 µL/well) and incubated the 96-well plate for 2 hours at room temperature. The 4G10 antibody was biotinylated with Sulfo-NHS®-Biotin according to the suppliers protocol (Pierce, USA) and purified by Micro Bio-Spin 6 chromatography columns (BIO RAD Laboratories, Inc., USA) using PBS as diluent. Plates were washed 5 times with PBS/0.05% Tween®20. Alkaline phosphatase-conjugated streptavidin SA110 (Millipore, USA) (1:4000) was used in PBS/0.05% Tween®20 + 10% FBS (100 µL/well) and incubated for 30 minutes at room temperature. Plates were washed 5 times with PBS/0.05% Tween®20. For fluorometric detection of alkaline phosphatase AttoPhos Substrate Set (Roche Diagnostics GmbH, Germany) was used (100 µL/well). The fluorometric signal was quantified after 90 minutes at a wavelength of 430/560 nm using a TECAN Ultra Evolution plate reader (Tecan Deutschland GmbH, Germany).

Kinase selectivity profiling

The kinase selectivity profiling was performed by Proteros Biostructures GmbH (Germany) according to the company`s standard operation procedure. The calculations of percent inhibition have been performed using three different types of assays, namely IMAP, binding, and HTRF assay. The experiments have been performed in triplicates.

IMAP assay

The IMAP assay (Molecular Devices) detects kinase activity in solution. A fluorescently-labeled substrate peptide is phosphorylated in the kinase reaction. After the reaction, a binding

solution containing large trivalent metal-based nanoparticles is added and the phosphorylated substrate binds to these beads. This reduces the rotational speed of the substrate which can be detected using fluorescence polarization. The following kinases were used: ABL, AKT1, AURA, AXL, CDK2, CDK4, CHK1, cKIT, c-MET, CSK, FGFR3, FLT3, IKKbeta, INSR, IRAK4, JAK3, JNK1, ERK1, PAK1, PAK4, PDGFRbeta, PIM1, PKCa, PLK3, Ret, RockII, SRC, SYC, TIE2, TRKA, VEGFR-2 and ZIPK.

Binding assay

The binding assay is based on reporter probes that are designed to bind to the site of interest of the target protein. The binding of the reporter probe to the protein results in the emission of an optical signal. Compounds that bind to the same site as the reporter probe displace the probe, causing signal diminution. Probe displacement is calculated in percent. Signal reflecting 100% probe displacement is determined in the absence of enzyme, while 0% probe displacement is measured in the absence of compound. The reporter probe is used at a concentration reflecting its own Kd (probe) value. The following kinases were used: BRAF, DDR1 and mTOR.

HTRF assay

This assay detects kinase activity with time resolved fluorescence transfer (TR-FRET). A biotinylated, kinase-specific peptide is phosphorylated in the kinase reaction. After the reaction, two detection reagents are added, first an antibody recognizing the phosphorylated amino acid residue which is labeled with europium cryptate as a FRET-donor, and second streptavidin which binds to the peptide via its biotin group and carries XL665 as a FRET-acceptor. If the substrate becomes phosphorylated, the close proximity between the FRET-

donor and -acceptor allow for the measurement of the TR-FRET signal. The HER2 kinase was analyzed by HTRF-assay.

KinAffinity:

To determine the quantitative kinase-target profile of these compounds, proprietary chemical proteomics methodologies and quantitative mass spectrometry were combined. The method was used as described by Sharma et al.[28] and Delehouzé et al.[29]. In brief, a total lysate of SILAC-labeled MDA-MB-231 cells was prepared. Subsequently, a matrix comprising immobilized broad-spectrum kinase inhibitors was used to enrich the expressed kinome of the cell sample. Competition assays with the free compounds and quantitative mass spectrometric analyses revealed the compounds' affinity profiles, ranking all kinase targets according to their Kd values for the free compounds. In summary, KinAffinity comprises five steps: a) cell culture; b) equilibrium binding of the target proteins to the KinAffinity matrix and the free test compound; c) differential chemical isotope labeling of proteins retained by the KinAffinity matrix; d) target identification and quantification by mass spectrometry; and e) data processing, curve fitting and target-affinity determination. Quantitative mass spectrometry requires the generation of differentially labeled protein samples. In the case of the MDA-MB-231 cells, this was achieved by stable isotope dimethyl labeling. The experimental setup of the chemical proteomics part was divided into two steps, both performed under equilibrium conditions. First, a lysate of MDA-MB-231 cells was applied to the KinAffinity matrix comprising different concentrations of various immobilized broadband kinase inhibitors, adjusted by dilution with control resin. These quantitative binding experiments allow one to determine the concentration of the immobilized compounds required to obtain 50% binding (BC_{50}) of each target protein to the matrix. Second, a lysate of the MDA-MB-231 cells was applied to the KinAffinity matrix with the highest loading density of

kinase inhibitors in the presence of increasing concentrations of the free compound **19h** or **19i**, respectively. These quantitative competition experiments determine the free compound concentration at which as many target proteins bind to the free compound as to the KinAffinity matrix (CC50). The final Kd values for the free compound are calculated for each target protein using the Cheng-Prusoff equation. Two quantitative competition experiments were performed in parallel to monitor whether equilibrium conditions were established. In the first experiment, the cell lysate was incubated with the free compound and the KinAffinity matrix was added subsequently. In the second experiment, the free compound and the KinAffinity matrix were added simultaneously. Under equilibrium conditions the competition curves from both experiments should be congruent for each target protein. Complete lists of all identified target kinases of **19h** and **19i** and of all kinases that bound to the KinAffinity matrix are included in the Supporting Information, Table S3.

Kinase interaction panel (DiscovRx KinomeScan 442 Kinases)

Assays were performed essentially as described previously by Fabian et al., [30] and Karaman et al., [31] and Wilson et al. [20].

ADME Assays

Chemicals and Instruments

All solvents, reagents, and l-α-phosphatidylcholine were purchased from Sigma-Aldrich Srl (Milan, Italy). Dodecane was purchased from Fluka (Milan, Italy). Pooled Male Donors 20 mg/mL HLM were from BD Gentest-Biosciences (San Jose, California). Milli-Q quality water (Millipore, Milford, MA, USA) was used. Hydrophobic filter plates (MultiScreen-IP, Clear Plates, 0.45 μm-diameter pore size), 96-well microplates, and 96-well UV-transparent microplates were obtained from Millipore (Bedford, MA, USA). LC analyses for the PAMPA

studies were performed with a Perkin-Elmer HPLC (series 200) equipped with an injector valve, a 20 μL sample loop (Mod. Rheodyne), and a UV detector (Perkin-Elmer 785A, UV/vis Detector). UV detection was monitored at 254 nm. LC analyses for the solubility and metabolic stability studies were performed with an Agilent 1100 LC/MSD VL system (G1946C) (Agilent Technologies, Palo Alto, CA) constituted by a vacuum solvent degassing unit, a binary high-pressure gradient pump, an 1100 series UV detector, and an 1100 MSD model VL benchtop mass spectrometer. The Agilent 1100 series mass spectra detection (MSD) single-quadrupole instrument was equipped with the orthogonal spray API-ES (Agilent Technologies, Palo Alto, CA). Nitrogen was used as nebulizing and drying gas. The pressure of the nebulizing gas, the flow of the drying gas, the capillary voltage, the fragmentor voltage, and the vaporization temperature were set at 40 psi, 9 L/min, 3000 V, 70 V, and 350°C, respectively. UV detection was monitored at 254 nm. The LC-ESI-MS determination was performed by operating the MSD in the positive ion mode. Spectra were acquired over the scan range m/z 100−1500 using a step size of 0.1 us.

Solubility Assay

Stock solutions of each compound in 10^{-3} M DMSO were prepared and sequentially diluted to reach the 10^{-6} M concentration. Four different aliquots (1.0, 1.5, 3.0, and 6.0 μL) of each 10^{-6} M stock solution of all compounds were dispensed into well plates with the necessary amount of water to reach the final volume of 300 μL. Wells were shaken in a shaker bath at room temperature for 24 h. These suspensions were filtered through a 0.45μm nylon filter (Acrodisc), proceeding with the chromatographic assays, performed in triplicate for each compound. Quantitative analysis was performed by means of the LC-UV method above-reported. LC analyses were conducted via HPLC (Agilent 1100 LC/MSD VL system) using a Varian Polaris 5 C18-A column (150 × 4.6 mm, 5 μm particle size) maintained at room

temperature at a flow rate of 0.8 mL/min with a mobile phase composed of 70% ACN/H_2O 30%.

Parallel Artificial Membrane Permeability Assay (PAMPA)

Donor solution (0.5 mM) was prepared by diluting 1 mM dimethyl sulfoxide (DMSO) compound stock solution using phosphate buffer (pH 7.4, 0.025 M). Filters were coated with 5 μL of a 1% (w/v) dodecane solution of phosphatidylcholine. Donor solution (150 μL) was added to each well of the filter plate. To each well of the acceptor plate were added 300 μL of solution (50% DMSO in phosphate buffer). All compounds were tested in three different plates on different days. The sandwich was incubated for 5 h at room temperature under gentle shaking. After the incubation time, the sandwich plates were separated, and samples were taken from both receiver and donor sides and analyzed using LC with UV detection. LC analyses were conducted via HPLC (Perkin-Elmer series 200) using a Polaris C18 column (150 × 4.6 mm, 5 μm particle size) at a flow rate of 0.8 mL/min with a mobile phase composed of 80% ACN/20% H_2O−formic acid 0.1%. Permeability (P_{app}) for PAMPA was calculated to obtain permeability values in cm/s: where VA is the volume in the acceptor well, VD is the volume in the donor well (cm^3), A is the "effective area" of the membrane (cm^2), t is the incubation time (s), and r is the ratio between drug concentration in the acceptor and equilibrium concentration of the drug in the total volume (VD + VA). Drug concentration is estimated by using the peak area integration.

Caco-2 Permeability Assay

Caco-2 cells, grown in tissue culture flasks, were trypsinized, resuspended, and grown and differentiated in 96-well plates for three weeks; monolayer formation was determined by measuring transport of Lucifer yellow, an impermeable dye. All assays were performed at a

concentration of 10 μM for 2 h. For apical to basolateral (A→B) permeability, compounds were added on the apical side (A), with permeation determined at the receiving (basolateral, B) side, where the receiving buffer was removed for analysis by LC/MS/MS using an Agilent 6410 mass spectrometer (ESI, MRM mode) coupled with an Agilent 1200 HPLC. Buffers used were 100 μM Lucifer yellow in transport buffer (1.98 g/L glucose in 10 mM HEPES, 1X Hank's balanced salt solution, pH 6.5) (apical side) and transport buffer, pH 7.4 (basolateral side). Apparent permeability (P_{app}) is expressed using the following equation: $P_{app} = (dQ/dt)/C_0A$, where the numerator is the rate of permeation, C_0 is initial concentration, and A is the monolayer area. For bidirectional permeability, the efflux ratio was defined as P_{app} (B→A)/P_{app} (A→B); high efflux ratio values (>3) indicate that a compound may be a substrate for P-gp or other active transport systems.

Microsomal Stability Assay

Each compound in DMSO solution was incubated at 37 °C for 60 min in 125 mM phosphate buffer (pH 7.4), 5 μL of human liver microsomal protein (0.2 mg/mL), in the presence of a NADPH-generating system at a final volume of 0.5 mL (compounds' final concentration, 100 μM); DMSO did not exceed 2% (final solution). The reaction was stopped by cooling in ice and adding 1.0 mL of acetonitrile. The reaction mixtures were then centrifuged, and the parent drug and metabolites were subsequently determined by LC-MS. Quantitative and qualitative analysis was performed by means of the LC-UV method above-reported. LC analyses were conducted via HPLC (Agilent 1100 LC/MSD VL system) using a Varian Polaris 5 C18-A column (150 × 4.6 mm, 5 μm particle size) maintained at room temperature. Chromatographic analysis was carried out using gradient elution with eluent A being ACN and eluent B consisting of an aqueous solution of formic acid (0.1%). The analysis started with 10% of eluent A, which was rapidly increased up to 70% in 10 min, then slowly increased up to 98%

in 15 min, and finally returned to 10% of eluent A in 1.0 min. The flow rate was 0.8 mL/min, and injection volume was 5 μL.

General Procedures for the Microsomal Stability Assay

All assays were conducted in duplicate. The incubation mixtures were prepared in E-tube and were contained with 5 μM synthesized analogue, 1 mg/mL liver microsomes (from mouse and human), and NADPH regeneration solution (1.3 mM NADP+, 3.3 mM glucose 6-phosphate, 3.3 mM $MgCl_2$, and 0.4 U/mL glucose 6-phosphate dehydrogenase) in 100 mM potassium phosphate buffer solution. Reactions were initiated by the addition of NADPH and kept in a shaking water bath at 37 °C. At the each sampling time, aliquots were removed and added to termination solvent (acetonitrile). The samples were centrifuged for 4–5 min at 13000 rpm, and the supernatant was subjected to HPLC analysis (HPLC/Agilent 1200 series). In the determination of the in vitro t1/2 (half-life, HL), the analyte peak areas were converted to percentage of drug remaining, using the T = 0 peak area values as 100%. The slope of the linear regression from log percentage remaining versus incubation time relationships (−k) was used in the conversion to the in vitro t1/2, values by the in vitro t1/2= −0.693/k. The percent remaining of test compound is calculated compared to the initial quantity at 0 time.

Pharmacokinetic Studies

Male mice (imprinting control region mice, body-weight range of 27 ± 5 g, iv, n = 3, po, n = 3) were administered intravenously via the tail vein at 2 and 1 mg/kg, respectively, or orally at 10 and 5 mg/kg, respectively, by gavage in a solution of 30% PEG400 and 5% ethanol in distilled water. At predetermined times 24 h or more after dosing, 0.3 mL blood was collected from the jugular vein using a tube containing anticoagulant (1000 IU/mL, heparin, 3 μL). The plasma was separated by centrifugation (12000 rpm, 2 min, Eppendorf). The concentrations

of the compound were measured in the plasma using LC/MS/MS after protein precipitation with acetonitrile. The relevant estimated pharmacokinetic parameters for plasma were derived using WinNonlin, version 5.2 (Pharsight).

Mouse studies

MDA-MB231 human breast tumors were orthotopically inoculated into female SCID/Beige mice (Harlan Laboratories, Inc, USA). MBA-MB231 human breast tumor cells were cultured in MEM cell culture medium, supplemented with 10% FBS, 1% Glutamax, 1% sodium pyruvate, NEAA and 1% penicillin-streptomycin. The cells were suspended in HBSS:MatrigelTM (1:1, v/v) to a final concentration of 4 x 10^7 cells/mL. The mice were anaesthetised with Ketamine (14 mg/mL) /Xylazine (0.9 mg/mL) prior to inoculation. The needle was introduced directly into the third mammary fat pad where 50 µL of cells (2 x 10^6 cells) were discharged. Vehicle Control (PEG400/H_20 (70:30 v/v), 19h (30 mg/kg) were administered twice daily (12 hours apart) via intra-peritoneal injection (ip). Paclitaxel (10 mg/kg) was administered three times weekly via intravenous injection (iv). 10 animals per group were used. Body weights were recorded for all animals three times per week. Tumor Measurements Tumor dimensions (length and diameter) were measured for all animals beginning when first palpable (day 12 of the study), and then three times per week. The tumor, lungs and regional lymph nodes (as many as could be found in each mouse) were excised from all mice. Lung surface and lung micro metastases were assessed. Lungs and lymph nodes were preserved in 10% neutral buffered formalin. Lymph nodes were embedded and sections were stained with Haematoxylin & Eosin (H&E) for assessment of tumor cell infiltration. Mean score ± SEM values of all lymph nodes in each group were calculated.

During the study, the care and use of animals was conducted in accordance with the principles outlined in the Guide for the Care and Use of Laboratory Animals, 8th Edition, 2010 (National

Research Council). All procedures used in the performance of this study were carried out in accordance with vivoPharm's Standard Operating Procedures.

ASSOCIATED CONTENT

AUTHOR INFORMATION

Corresponding author

*Phone: +36-30-2316885. Fax: +36-1-4872081. E-mail: orfi.laszlo@pharma.semmelweis-univ.hu

Author Contributions

⊥These authors contributed equally to this work.

Notes

The authors declare no competing financial interest.

ACKNOWLEDGMENTS

The research leading to these results was supported by the Max-Planck Society. The authors thank to Servier Research Institute of Medicinal Chemistry (Budapest), for the HRMS measurements and to Dr. András Dancsó (EGIS Pharmaceuticals PLC) for his help in the molecular modeling and pharmacophore model generation.

ABBREVIATIONS

DIPEA, N,N-diisopropylethylamine; DFG, Asp (D) - Phe (F) - Gly (G) residues of the activation loop; IMAP, Immobilized Metal Assay for Phosphochemicals, MXT, mammary tumor xenograft model. The full names of abbreviated kinases mentioned in the manuscript can be found in the Supporting Information, Table S4 (page S154).

Supporting Information

The Supporting Information is available free of charge via the Internet at http://pubs.acs.org. Detailed synthesis procedures and characterization data for all compounds, 1D and correlation NMR spectra for the selected compounds (**18d, 19e, 19h, 19i, 20b, 20g, 21f**). DiscoveRx Kinomescan Kinase Selectivity Panel (442 kinases) at 5μM concentration for **20b** and **20g** (Table S1 and S2). Complete lists of all kinases that bound to the KinAffinity matrix and of all identified target kinases (Table S3). Molecular formula strings including AXL IC_{50} values (CSV).

REFERENCES

(1) O'Bryan, J. P.; Frye, R. A.; Cogswell, P. C.; Neubauer, A.; Kitch, B.; Prokop, C.; Espinosa, R., 3rd; Le Beau, M. M.; Earp, H. S.; Liu, E. T. AXL, a transforming gene isolated from primary human myeloid leukemia cells, encodes a novel receptor tyrosine kinase. *Mol. Cell. Biol.,* **1991**, *11*, 5016-5031.

(2) Janssen, J. W.; Schulz, A. S.; Steenvoorden, A. C.; Schmidberger, M.; Strehl, S.; Ambros, P. F; Bartram, C. R. A novel putative tyrosine kinase receptor with oncogenic potential. *Oncogene,* **1991**, *6*, 2113-2120.

(3) Paccez, J. D.; Vogelsang, M.; Parker, M. I.; Zerbini, L. F. The receptor tyrosine kinase AXL in cancer: Biological functions and therapeutic implications. *Int. J. Cancer.,* **2014** *134(5)*, 1024-33. DOI: 10.1002/ijc.28246. Published online: June 4, 2013.

(4) Stitt, T. N.; Conn, G.; Gore, M.; Lai, C.; Bruno, J.; Radziejewski, C.; Mattsson, K.; Fisher, J.; Gies, D. R, Jones, P. F.; Masiakowski, P.; Terence, E. R.; Nancy, J. T.; Chen,

D. H.; DiStefano, P. S.; Long, G. L.; Basilico, C.; Goldfarb, M. P.; Lemke, G.; Glass, D. J.; Yancopoulos, G. D. The anticoagulation factor protein S and its relative, Gas6, are ligands for the Tyro3/AXL family of receptor tyrosine kinases. *Cell,* **1995**, *80*, 661-670.

(5) Goruppi, S.; Ruaro, E.; Varnum, B.; Schneider, C. Requirement of phosphatidylinositol 3-kinase-dependent pathway and Src for Gas6-AXL mitogenic and survival activities in NIH3T3 fibroblasts. *Mol. Cell. Biol.,* **1997**, *17*, 4442-4453.

(6) Demarchi, F.; Verardo, R.; Varnum, B.; Brancolini, C.; Schneider, C. Gas6 anti-apoptotic signaling requires NF-kappa B activation. *J. Biol. Chem.,* **2001**, *276*, 31738-31744.

(7) Goruppi, S.; Ruaro, E.; Schneider, C. Gas6, the ligand of AXL tyrosine kinase receptor, has mitogenic and survival activities for serum starved NIH3T3 fibroblasts. *Oncogene,* **1996**, *12*, 471-480.

(8) Yanagita, M.; Arai, H.; Nakano, T.; Ohashi, K.; Mizuno, K.; Fukatsu, A.; Doi, T.; Kita, T. Gas6 induces mesangial cell proliferation via latent transcription factor STAT3. *J. Biol. Chem.,* **2001**, *276*, 42364-42369.

(9) Holland, S. J.; Powell, M. J.; Franci, C.; Chan, E. W.; Friera, A. M.; Atchison, R. E.; McLaughlin, J.; Swift, S. E.; Pali, E. S.; Yam, G.; Wong, S.; Lasaga, J.; Shen, M. R.; Yu, S.; Xu, W.; Hitoshi, Y.; Bogenberger, J.; Nor, J. E.; Payan, D. G.; Lorens, J. B. Multiple roles for the receptor tyrosine kinase AXL in tumor formation. *Cancer Res.,* **2005**, *65*, 9294-9303.

(10) Dufies, M.; Jacquel, A.; Belhacene, N.; Robert, G.; Cluzeau, T.; Luciano, F.; Cassuto, J. P.; Raynaud, S.; Auberger, P. Mechanisms of AXL overexpression and function in imatinib-resistant chronic myeloid leukemia cells. *Oncotarget,* **2011**, *2*, 874-885.

(11) Mahadevan, D.; Cooke, L.; Riley, C.; Swart, R.; Simons, B.; Della Croce, K.; Wisner, L.; Iorio, M.; Shakalya, K.; Garewal, H.; Nagle, R.; Bearss, D. A novel tyrosine kinase switch is a mechanism of imatinib resistance in gastrointestinal stromal tumors. *Oncogene,* **2007**, *26*, 3909-3919.

(12) Zhang Y. X.; Knyazev, P. G.; Cheburkin, Y. V.; Sharma, K.; Knyazev, Y. P.; Őrfi, L.; Szabadkai, I.; Daub, H.; Kéri, G.; Ullrich, A. AXL is a potential target for therapeutic intervention in breast cancer progression. *Cancer Res.,* **2008**, *68*, 1905-1915.

(13) Liu, L.; Greger, J.; Shi, H.; Liu, Y.; Greshock, J.; Annan, R.; Halsey, W.; Sathe, G. M.; Martin, A. M.; Gilmer, T. M. Novel mechanism of lapatinib resistance in HER2-positive breast tumor cells: activation of AXL. *Cancer Res.,* **2009**, *69*, 6871-6878.

(14) Schroeder, G. M.; An, Y.; Cai, Z. W.; Chen, X. T.; Clark, C.; Cornelius, L. A.; Dai, J.; Gullo-Brown, J.; Gupta, A.; Henley, B.; Hunt, J. T.; Jeyaseelan, R.; Kamath, A.; Kim, K.; Lippy, J.; Lombardo, L. J.; Manne, V.; Oppenheimer, S.; Sack, J. S.; Schmidt, R. J.; Shen, G.; Stefanski, K.; Tokarski, J. S.; Trainor, G. L.; Wautlet, B. S.; Wei, D.; Williams, D. K.; Zhang, Y.; Zhang, Y.; Fargnoli, J.; Borzilleri, R. M. Discovery of N-(4-(2-amino-3-chloropyridin-4-yloxy)-3-fluorophenyl)-4-ethoxy-1-(4-fluorophenyl)-2-oxo-1,2-dihydropyridine-3-carboxamide (BMS-777607), a selective and orally

efficacious inhibitor of the MET kinase superfamily. *J. Med. Chem.,* **2009**, *52*, 1251-1254.

(15) Yakes, F. M.; Chen, J.; Tan, J.; Yamaguchi, K.; Shi, Y.; Yu, P.; Qian, F.; Chu, F.; Bentzien, F.; Cancilla, B.; Orf, J.; You, A.; Laird, A. D.; Engst, S.; Lee, L.; Lesch, J.; Chou, Y. C.; Joly, A. H. Cabozantinib (XL184), a novel MET and VEGFR2 inhibitor, simultaneously suppresses metastasis, angiogenesis, and tumor growth. *Mol. Cancer Ther.,* **2011**, *10*, 2298-2308.

(16) Burbridge, M. F.; Bossard, C. J.; Saunier, C.; Fejes, I.; Bruno, A.; Léonce, S.; Ferry, G.; Da Violante, G.; Bouzom, F.; Cattan, V.; Jacquet-Bescond, A.; Comoglio, P. M.; Lockhart, B. P.; Boutin, J. A.; Cordi, A.; Ortuno, J. C.; Pierré, A.; Hickman, J. A.; Cruzalegui, F. H.; Depil, S. S49076 is a novel kinase inhibitor of MET, AXL, and FGFR with strong preclinical activity alone and in association with bevacizumab. *Mol. Cancer Ther.,* **2013**, *12*, 1749-1762.

(17) Holland, S. J.; Pan, A.; Franci, C.; Hu, Y.; Chang, B.; Li, W.; Duan, M.; Torneros, A.; Yu, J.; Heckrodt, T. J.; Zhang, J.; Ding, P.; Apatira, A.; Chua, J.; Brandt, R.; Pine, P.; Goff, D.; Singh, R.; Payan, D. G.; Hitoshi, Y. R428, a selective small molecule inhibitor of AXL kinase, blocks tumor spread and prolongs survival in models of metastatic breast cancer. *Cancer Res.,* **2010**, *70*, 1544-1554.

(18) Kéri, G.; Székelyhidi, Z.; Bánhegyi, P.; Varga, Z.; Hegymegi-Barakonyi, B.; Szántai-Kis, C.; Hafenbradl, D.; Klebl, B.; Muller, G.; Ullrich, A.; Erös, D.; Horváth, Z.; Greff, Z.; Marosfalvi, J.; Pató, J.; Szabadkai, I.; Szilágyi, I.; Szegedi, Z.; Varga, I.; Wáczek, F.;

Őrfi, L. Drug discovery in the kinase inhibitory field using the Nested Chemical Library technology. *Assay Drug Dev. Technol.,* **2005**, *3*, 543-551.

(19) Kubo, K.; Shimizu, T.; Ohyama, S.; Murooka, H.; Iwai, A.; Nakamura, K.; Hasegawa, K.; Kobayashi, Y.; Takahashi, N.; Takahashi, K.; Kato, S.; Izawa, T.; Isoe, T. Novel potent orally active selective VEGFR-2 tyrosine kinase inhibitors: synthesis, structure-activity relationships, and antitumor activities of N-phenyl-N'-{4-(4-quinolyloxy)phenyl}ureas. *J. Med. Chem.,* **2005**, *48*, 1359-1366.

(20) Wilson C, Ye X, Pham T, Lin E, Chan S, McNamara E, Neve RM, Belmont L, Koeppen H, Yauch RL, Ashkenazi A, Settleman J. AXL inhibition sensitizes mesenchymal cancer cells to antimitotic drugs. *Cancer Res.,* **2014**, *74(20)*, 5878-5890.

(21) D'Alfonso, T.M.; Hannah, J.; Chen, Z.; Liu, Y.; Zhou, P.; Shin, S.J. AXL receptor tyrosine kinase expression in breast cancer. *J. Clin. Pathol*., **2014**, *67*, 690-696.

(22) Ren, D.;, Li, Y.; Gong, Y.; Xu, J.; Miao, X.; Li, X.; Liu, C.; Jia, L.; Zhao, Y. Phyllodes tumor of the breast: role of AXL and ST6GalNAcII in the development of mammary phyllodes tumors. *Tumor Biol.,* **2014**, *35*, 9603-9612.

(23) Pénzes K, Baumann C, Szabadkai I, Őrfi L, Kéri G, Ullrich A, Torka R., Combined inhibition of AXL, LYN and p130Cas kinases block migration of triple negative breast cancer cells. *Cancer Biol Ther*. **2014**, *15(11)*, 1571-1582

(24) Uribe DJ, Mandell EK, Watson A, Martinez JD, Leighton JA, Ghosh S. The receptor tyrosine kinase AXL promotes migration and invasion in colorectal cancer. *PLoS ONE*, **2017**, *12(7)*, Published: July 20, 2017, https://doi.org/10.1371/journal.pone.0179979.

(25) Leconet W, Chentouf M, du Manoir S, Chevalier C, Sirvent A, Aït-Arsa I, Busson M, Jarlier M, Radosevic-Robin N, Theillet C, Chalbos D, Pasquet JM, Pèlegrin A, Larbouret C, Robert B. Therapeutic activity of anti-AXL antibody against triple-negative breast cancer patient-derived xenografts and metastasis. *Clin Cancer Res*., 2017, *23(11)*, 2806-2816.

(26) Cerchia L, Esposito CL, Camorani S, Rienzo A, Stasio L, Insabato L, Affuso A, de Franciscis V. Targeting Axl with an high-affinity inhibitory aptamer. *Mol Ther*., **2012**, *20(12)*, 2291-2303.

(27) Paolino M, Choidas A, Wallner S, Pranjic B, Uribesalgo I, Loeser S, Jamieson AM, Langdon WY, Ikeda F, Fededa JP, Cronin SJ, Nitsch R, Schultz-Fademrecht C, Eickhoff J, Menninger S, Unger A, Torka R, Gruber T, Hinterleitner R, Baier G, Wolf D, Ullrich A, Klebl BM, Penninger JM. The E3 ligase Cbl-b and TAM receptors regulate cancer metastasis via natural killer cells. *Nature*, **2014**, *507(7493)*, 508-512.

(28) Sharma K, Weber C, Bairlein M, Greff Z, Kéri G, Cox J, Olsen JV, Daub H. Proteomics strategy for quantitative protein interaction profiling in cell extracts. *Nat. Methods*., **2009**, *6(10)*, 741-744. doi: 10.1038/nmeth.1373. Epub 2009 Sep 13.

(29) Delehouzé C, Godl K, Loaëc N, Bruyère C, Desban N, Oumata N, Galons H, Roumeliotis T, Giannopoulou EG, Grenet J, Twitchell D, Lahti J, Mouchet N, Galibert MD, Garbis SD, Meij. CDK/CK1 inhibitors roscovitine and CR8 downregulate amplified MYCN in neuroblastoma cells. *Oncogene*, **2014**, *33(50)*, 5675-5687.

(30) Fabian MA, Biggs WH, Treiber DK, Atteridge CE, Azimioara MD, Benedetti MG Carter TA, Ciceri P, Edeen PT, Floyd M, Ford JM, Galvin M, Gerlach JL, Grotzfeld RM, Herrgard S, Insko DE, Insko MA, Lai AG, Lélias JM, Mehta SA, Milanov ZV, Velasco AM, Wodicka LM, Patel HK, Zarrinkar PP, Lockhart DJ. A small molecule-kinase interaction map for clinical kinase inhibitors. *Nat. Biotechnol.,* **2005**, *23,* 329-336.

(31) Karaman MW, Herrgard S, Treiber DK, Gallant P, Atteridge CE, Campbell BT, Chan KW, Ciceri P, Davis MI, Edeen PT, Faraoni R, Floyd M, Hunt JP, Lockhart DJ, Milanov ZV, Morrison MJ, Pallares G, Patel HK, Pritchard S, Wodicka LM, Zarrinkar PP. A quantitative analysis of kinase inhibitor selectivity. *Nat. Biotechnol.,* **2008**, *26*, 127-132.

Table of Contents graphic

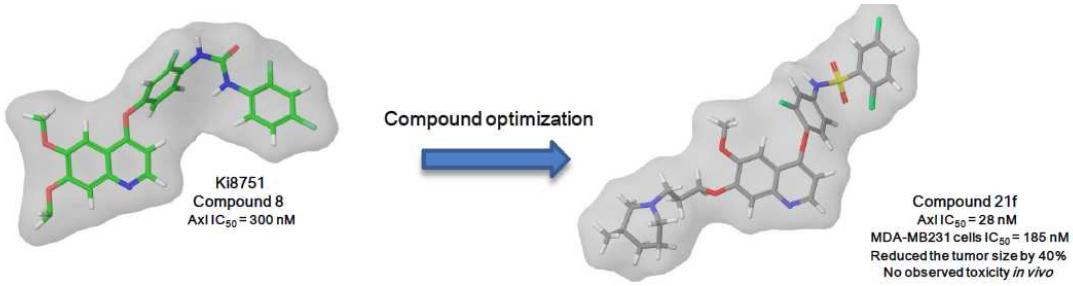

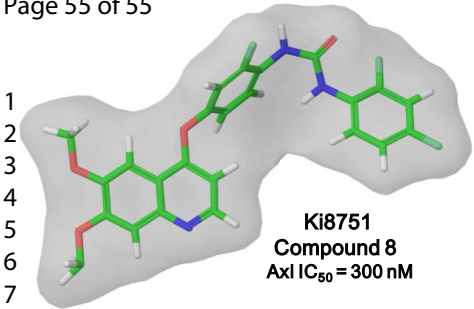

Ki8751
Compound 8
Axl IC_{50} = 300 nM

Compound optimization

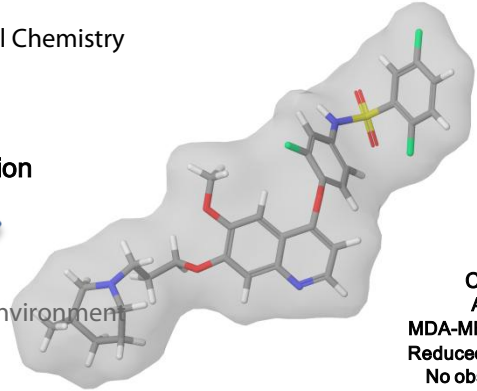

Compound 21f
Axl IC_{50} = 28 nM
MDA-MB231 cells IC_{50} = 185 nM
Reduced the tumor size by 40%
No observed toxicity *in vivo*